3-6 Mineralization in the Survey Area and Ore Deposits in the Vicinity

The type, host rocks, age, alteration, and results of fluid inclusion studies of the mineralization of the North Prospect, the South Prospect, and the 4/6 Gossan in the survey area and Jabal Sayid deposit and Mahd adh Dhahab mine in the neighboring areas were compared (Table 2-3-6).

(1) Mineralization type

The mineralization of the three known prospects in the survey area is disseminated to network-type copper mineralization. And the 4/6 Gossan has high gold, silver, lead and zinc content. The Jabal Sayid deposit consists of stratabound massive copper sulfide mineralization with stockwork in the lower parts. The Mahd adh Dhahab mine was formed by vein-type Au-Ag-Cu-Zn mineralization.

(2) Host rocks

The ores of the three known prospects in the survey area are hosted by felsic rocks of the Arj Group. The host rocks of the Jabal Sayid deposit is felsic rocks of the Sayid Formation of the Arj Group. The deposits of the Mahd adh Dhahab mine occur in andesite and andesitic volcaniclastics of the Haf Formation of the Mahd Group.

(3) Age of mineralization

Mineralized zones of the three prospects lie in the shear zones within rhyodacite, dacite, and their volcaniclastic rocks, and the mineralization is not confirmed in andesite and its volcaniclastic rocks of the Arj Group, and intrusive bodies. Therefore, the mineralization is considered to have occurred after deposition of silicic rocks and before intrusion of diorite and tonalite. The mineralization of the Jabal Sayid deposit occurred at the time of the deposition of the Sayid Formation. On the other hand, the age of the mineralization of the Mahd adh Dhahab mine has been determined to be 649 Ma (DGMR, 1994). Probably, this corresponds to the time of deposition of the Ghamr Group overlying the Mahd Group.

(4) Ore minerals

The ore minerals of the North Prospect, Jabal Sayid deposit, and Mahd adh Dhahab mine are listed in Table 2-1-3. High temperature sulfides such as pyrrhotite, magnetite, and cubanite are observed in the North Prospect and the Jabal Sayid deposit, but these minerals have not been reported from the Mahd adh Dhahab mine.

(5) Alteration

The host rocks of the three prospects, the Jabal Sayid deposit, and the Mahd adh Dhahab mine have been silicified, chloritized and pyritized. The major difference in alteration is that potassium feldspar replacement is observed at Mahd adh Dhahab mine and large crystals of potassium feldspars, several centimeters in size, occur in the andesitic host rock, but these do not occur in the three prospects and the Jabal Sayid deposit.

(6) Fluid inclusions

The fluid inclusion study of the Mahd adh Dhahab mine has been reported by Luce et al., (1979), Rye et al., (1982), Hakim and Chinkul (1989) , and Afifi (1992). Luce et al., (1979) reported that the homogenization temperature of primary and pseudosecondary fluid inclusions in many kinds of quartz veins was 142° —278° C, and the salinity was 0—0.1 wt % NaCl. And the homogenization temperature of fluid inclusions in quartz has been reported to be 110° —238° C by Rye et al., (1982). Hakim and Chinkul (1989) stated that the homogenization temperature of fluid inclusions in mineralized quartz veins was 100° —380° C, and the salinity was 1—4 wt % NaCl, on the other hand, that of fluid inclusions in barren quartz veins was 130° —200° C, and the salinity was 0.6—3 wt % NaCl. Afifi (1992) determined that the temperature during hydrothermal activity at the Mahd adh Dhahab mine was 180° —270° C.

The fluid inclusion study of the Jabal Sayid deposit has been reported by Chinkul (1983). Chinkul (1983) indicated that the homogenization temerature of fluid inclusions in mineralized quartz veins and sphalerites was 300° —400° C, and the salinity was high as 6.7—7.4 wt % NaCl.

During the present survey, homogenization temperature and salinity of 14 quartz samples were measured. The samples are; 1 from the Jabal Sayid deposit, 2 from the Mahd adh Dhahab mine, 5 from the North Prospect, 3 from the South Prospect, 2 from Southeast Extension located southwest of the South Prospect, and 1 from north of the South Prospect. The measurement results are shown in Table 2-3-5.

The homogenization temperature is normally measured on primary fluid inclusions. But the inclusions measured during this work were very small, and distinction of primary and secondary inclusions was not possible, because of the following reasons.

① Growth bands of quartz were not observed, thus primary and secondary cannot be

distinguished by the texture.

② In samples on which relatively large number of measurements were made, fluid inclusions exist close to each other. This indicates the possibility of necked down fluids or secondary fluid inclusions.

③ The data of fluid inclusions which have planar arrangement and clearly of secondary origin and those without such arrangements are similar.

Therefore, the reliability of the homogenization temperature and salinity measured during this phase is not high.

The homogenization temperatures and salinities reported by Chinkul (1983) regarding the Jabal Sayid deposit, by Luce et al., (1979), and Hakim and Chinkul (1989) regarding the Mahd adh Dhahab mine, and by the present study are plotted in Figure 2-3-9.

The average homogenization temperature of the silicified ore sample (K9030307) collected from the stockpile of the Jabal Sayid deposits was 260° C, and the average salinity was 8.3 wt % NaCl. This temperature was slightly lower than that of Chinkul (1983), and the salinity is almost the same with that of Chinkul (1983). The average homogenization temperature and salinity of the two samples collected from the Mahd adh Dhahab mine were 210° C and 0.9 wt % NaCl for sample K9030308, and 192° C and 0.2 wt % NaCl for K9030309. These data are almost similar to those of Luce et al., (1979), and Hakim and Chinkul (1989).

The average homogenization temperature of the three samples collected from the South Prospect was 148° —164° C, and the average salinity was 3.2—5.0 wt % NaCl. The temperature is resemble to that of the Mahd adh Dhahab mine more than that of the Jabal Sayid deposit, but the salinity is relatively high. Of five samples collected from the North Prospect, the homogenization temperature and salinity could be measured for the three samples. The average salinities are higher than that of the South Prospect, and the average homogenization temperature is low contrary to the Jabal Sayid deposits.

(7) Discussions

It is concluded that the mineralization of the three prospects is epigenetic dissemination to network-type hydrothermal and it occurred within the shear zone formed by the tectonic

movement before the deposition of the Mahd Group. This is clearly different from the stratabound sulfide copper mineralization of the Jabal Sayid deposit and the younger Au-Ag-Cu-Zn mineralization of the Mahd adh Dhahab mine.

However, there are some points of similarity between the mineralization of the known mineral prospects in the survey area, the Jabal Sayid deposits, and the Mahd adh Dhahab mine. For example, occurrence of high-temperature sulfides such as pyrrhotite, magnetite, and cubanite is reported from the North Prospect and the Jabal Sayid deposit, and gold and silver contents of the mineralized zone of the 4/6 Gossan are high similar to those of the Mahd adh Dhahab mine. Therefore, it will be necessary to accumulate the data of core observation, microscopic observation of polished sections, absolute age determination, and X-ray diffraction analysis, and then to correlate mineralization of the known three prospects, the Jabal Sayid deposit, and the Mahd adh Dhahab mine.

Table 2-3-5 Results of Fluid Inclusion Study

Localities		Sample No.	Rock Name	Kind of Inclusions	Homogenization Temperature(℃)					Salinity (wt% eq. NaCl)					Other Analytical Results		
					Number of Measured Inclusions	Min	Max	Average	Standard Deviation	Number of Measured Inclusions	Min	Max	Average	Standard Deviation	Microscopic Observation of Polished Section	Ore Assay	X-ray Diffraction Analysis
Jabal Sayid Deposit		K9030307	silicified ore	liquid-rich two-phase	22	111	309	260	47	5	0.7	10.9	8.3	1.7	py(◎), cp(○), sp(△), po(△)	-	-
Mahd adh Dhahab Mine		K9030308	988mL,cp-sp qz vein	liquid-rich two-phase	15	147	276	221	46	14	0.6	1.2	0.9	0.2	py(△), cp(○), bn(△), sp(◎), ga(△)	-	-
		K9030309	quartz vein	liquid-rich two-phase	12	174	233	198	19	5	0.1	0.4	0.2	0.2	-	-	qz(◎), chl(◎), ser(△), epi(△), py(○), cp(○)
Umm ad Damar		K9022006	quartz vein	liquid only	0	-	-	-	-	2	12.3	14.4	13.3	1.5	-	Cu 1.48%	-
Umm ad Damar North Prospect	West Hill	K9030102	gossan	liquid only	0	-	-	-	-	3	11.7	12.5	12.2	0.4	py(△), hem(◎)	Cu 0.14%	-
		K9030103	quartz vein	mostly liquid-rich two-phase	11	172	240	193	31	11	4.9	7.3	6.2	0.9	-	Ag 18.9g/t, Cu 0.17%	-
	Southeast Hill	K9030301	sulfide veinlet ore, UAD-6 NO.17	liquid-rich two-phase	1	>430		-	-	1	6.0		-		py(◎), cp(○), sp(△), po(△), mt(△), cv(△)	Cu 0.19%	qz(○), chl(◎), py(△)
	Southeast Extension	K9022501	quartz vein	liquid only or liquid-rich two-phase	2	147	175	161	20	3	13.1	13.5	13.4	0.2	-	Cu 0.11%	-
		K9022505	silicified ore	liquid-rich two-phase	10	147	191	164	14	4	12.4	18.4	14.7	2.8	-	Cu 0.60%	-
Umm ad Damar South Prospect		K9022402	silicified rock	liquid-rich two-phase	20	150	181	160	12	5	1.5	4.1	3.2	1.0	-	-	-
		K9022403	qz-hem veinlet rock	liquid-rich two-phase	19	149	191	164	12	5	3.9	4.9	4.4	0.4	-	Cu 0.06%	-
		K9022406	silicified ore	liquid-rich two-phase	23	132	175	148	12	6	3.6	5.6	5.0	0.7	-	Ag 18.2g/t, Cu 1.91%	-
Umm ad Damar South Southeast Extension		K9021402	quartz vein	liquid only	0	-	-	-	-	1	0.5		-	-	-	Cu 0.45%	-
		K9021404	quartz vein	liquid-rich two-phase(CO_2?)	2	81	90	85	6	0	-	-	-	-	-	Cu 0.45%	-

abbrev. py = pyrite, cp = chalcopyrite, sp = sphalerite, po = pyrrhotite, bn = bornite, ga = galena, hem = hematite, mt = magnetite, cv = covelline, qz = quartz, chl = chlorite, ser = sericite, epi = epidote
◎abundant, ○common, △small

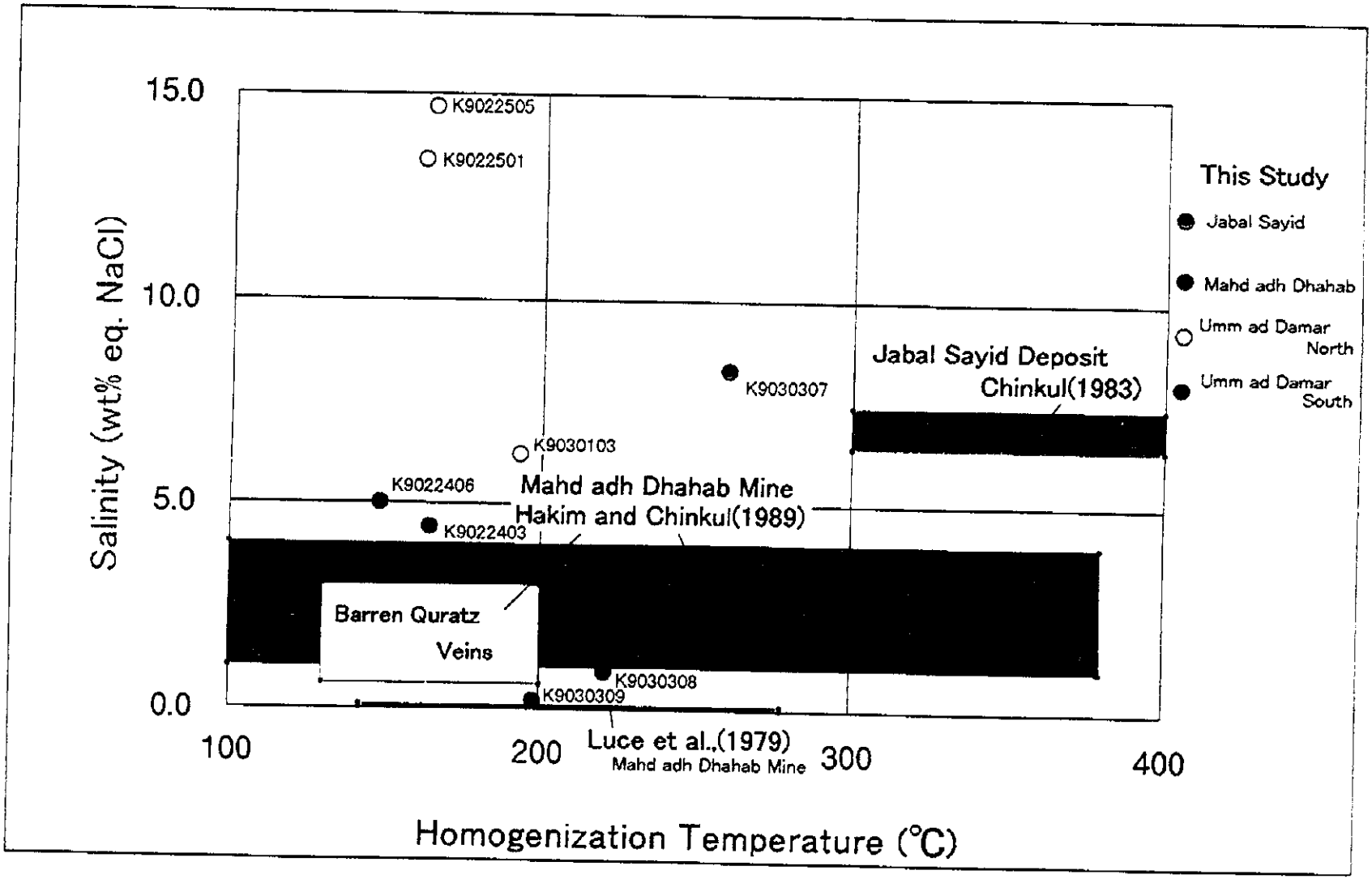

Fig. 2-3-9 Crossplots of Homogenization Temperature and Salinity of Fluid Inclusions

Table 2-3-6 Correlation of Mineral Prospects

	Umm ad Damar North Prospect	Umm ad Damar South Prospect	4/6 Gossan Prospect	Jabal Sayid deposit	Mahd adh Dhahab mine
Mineralization type	Disseminated and network-type Cu mineralization in shear zone	Disseminated and network-type Cu-(Au?) mineralization in shear zone	Au-Ag-Cu-Pb-Zn mineralization in shear zone	Stratabound massive sulfide type Cu mineralization	Vein type Au-Ag-Cu-Zn mineralization
Host rocks	Rhyodacite and dacite of Arj Group	Rhyodacite, andesite, andesitic tuff and dacitic tuff of Arj Group	Dacite, dacitic tuff and rhyodacite of Arj Group	Sayid Formation, Arj Group	Haf Formation, Mahd Group
Mineralization age	After deposition of silicic rocks and before intrusion diorite and tonalite			Sayid Formation deposition time	649 Ma (DGMR, 1994)
Alteration	Quartz-chlorite-pyrite	Quartz-chlorite-pyrite	Quartz-chlorite-pyrite	Quartz-chlorite-pyrite	Quartz-pyrite-chlorite-potassium feldspar
Fluid inclusion study	This study: 193℃ , 6.2wt%/ 161℃, 13.4wt%/ 164℃, 14.7wt%	This study: 160℃, 3.2wt%/ 164℃, 4.4wt%/ 148℃, 5.0wt%	Unknown	This study: 260℃, 8.3wt% Chinkul(1983): 300-400℃, 6.7-7.4wt	This study: 221℃, 0.9wt%/ 198℃, 0.2wt% Luce et al.,(1979): 142-278℃, 0-0.1wt% Hakim and Chinkul(1989): 100-380℃, 1-4wt%

CHAPTER 4 GEOPHYSICAL SURVEY

4-1 Outline of the Survey

(1) Objectives

The objectives of the geophysical survey using time domain IP method are to extract IP anomalies related to mineralization in the Umm ad Damar area (Fig.1-1).

(2) Exploration Method

Time domain IP method

(3) Amounts of Geophysical Survey

Amounts of geophysical survey are as follows.

- Field survey

Total length of lines	55 km
Survey lines	17 lines
Measuring points	1,962 points

- Laboratory test 36 pieces

4-2 Survey Method

4-2-1 Methodology

The IP method is the exploration method to observe electric polarization effect (IP effect) in the earth. The IP effect is caused by the following phenomena.

When direct current flows through the rocks containing metallic minerals, electric potential difference is generated between the surface of metallic minerals and pore water around it. This electric potential causes a store of electric charge and induces electric polarization. The electric charge is discharged gradually after current is cut off. It forms the residual voltage decaying with the passage of time. However, the IP effect occurs not only in the rocks containing metallic minerals, but also in some sedimentary rocks containing graphite or clay.

In the time domain IP method, on and off altemating current in the shape of rectangular wave, as shown in Figure 2-4-1, is generally used as transmitter current. Received voltage is

composed of the primary voltage Vp observed during current on and the decay voltage (secondary voltage Vs) observed during current off. Chargeability is calculated with received voltage as index to express quantity of IP effect. The chargeability M is defined in the following equation. It is the proportion of time integral of secondary voltage to primary voltage. Its unit is mV/V.

$$M = 1/Vp/(t2 - t1) \cdot \int_{t1}^{t2} Vs \; dt \qquad (4\text{-}1)$$

t1: Time at the beginning of Vs integration

t2: Time at the end of Vs integration

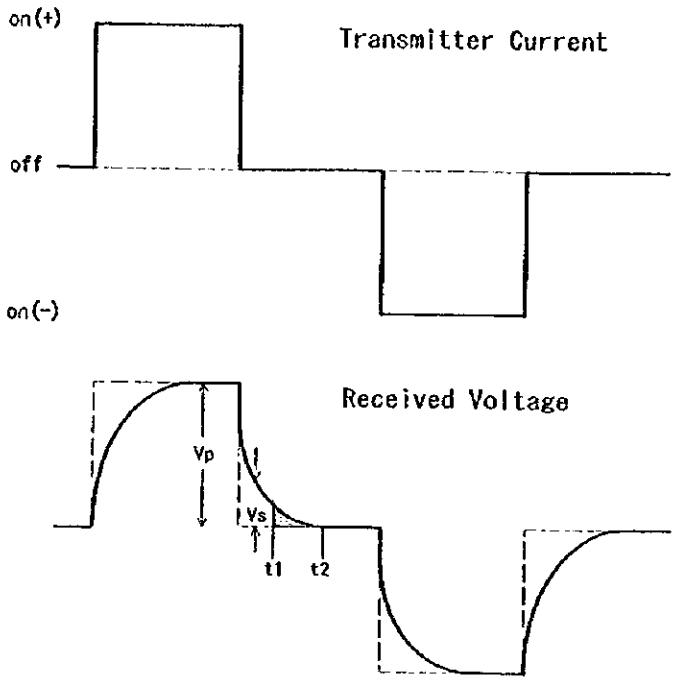

Fig. 2-4-1 Wave Form of Transmitter Current and Received Voltage

4-2-2 Field survey

The survey lines (300m interval) are laid out as shown in Figure 2-4-2. The lengths of the survey lines are shown in Table 2-4-1. The specifications of measurement are as follows.

Electrode configuration	:	Dipole-dipole array
Interval of measuring points	:	100 m
Electrode separation index	:	1 to 4
Electrode spacing	:	100 m
Observed quantity	:	Electric potential and chargeability
ON / OFF time	:	2 s
Time at the beginning of Vs measurement	:	450 ms
Time at the end of Vs measurement	:	1,100 ms

The equipment used in this survey are shown in Table 2-4-2.

4-2-3 Laboratory tests

Resistivity and chargeability of rock samples in the survey areas were measured in laboratory. The same method as in the field measurement was applied. Thirty six samples were measured in laboratory.

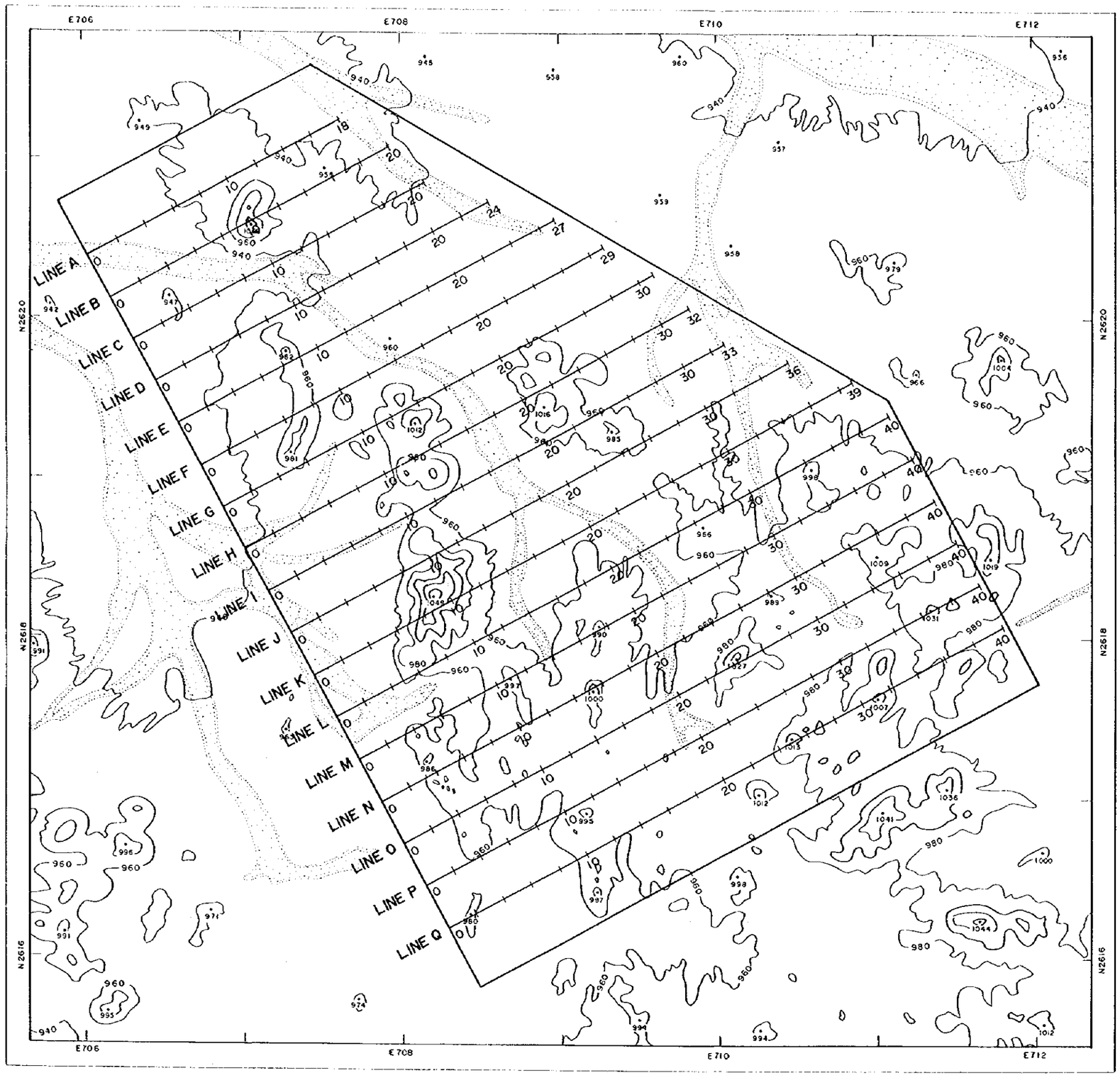

Scale 1:25,000

0 500 1,000 1,500m

Fig. 2-4-2 Location Map of the Survey Lines

Table 2-4-1 List of IP Survey Lines

Line	Length(km)	Amount of Measuring Points
A	1.8	58
B	2.0	66
C	2.1	70
D	2.4	82
E	2.7	94
F	2.9	102
G	3.1	110
H	3.2	114
I	3.3	118
J	3.6	130
K	3.9	142
L	4.0	146
M	4.0	146
N	4.0	146
O	4.0	146
P	4.0	146
Q	4.0	146
Total	55.0	1,962

Table 2-4-2 List of IP Survey Equipment

ITEM	MODEL	SPECIFICATION
Transmitter	Chiba CH-96T Transmitter Chiba CH-96A Power Controller	Output Voltage : 70, 120, 180, 250, 330 420, 520, 630, 750, 880 V Output Current : 0～15 A Wave Form : Rectangular Wave Frequency Range : DC～10,000 Hz Weight : 67 kg
Engine Generator	Honda ET4500 Engine Generator (2pcs)	Output Power : 4.5 kW Output Voltage : 200 V Weight : 78 kg
Receiver	Scintrex Time Domain IP/Resistivity Receiver	On/Off Time : 1, 2, 4, 8, 16, 32 s Resolution (VP) : 10 μV Resolution (M) : 0.01 mV/V Power : 12V Battery Weight : 5.8 kg
Electrode		Current : Stainless Rod Potential : Non Polarization CuSO4 Porous Pot

4-2-4 Analytical method

The analysis was carried out according to the flow chart as shown in Figure 2-4-3.

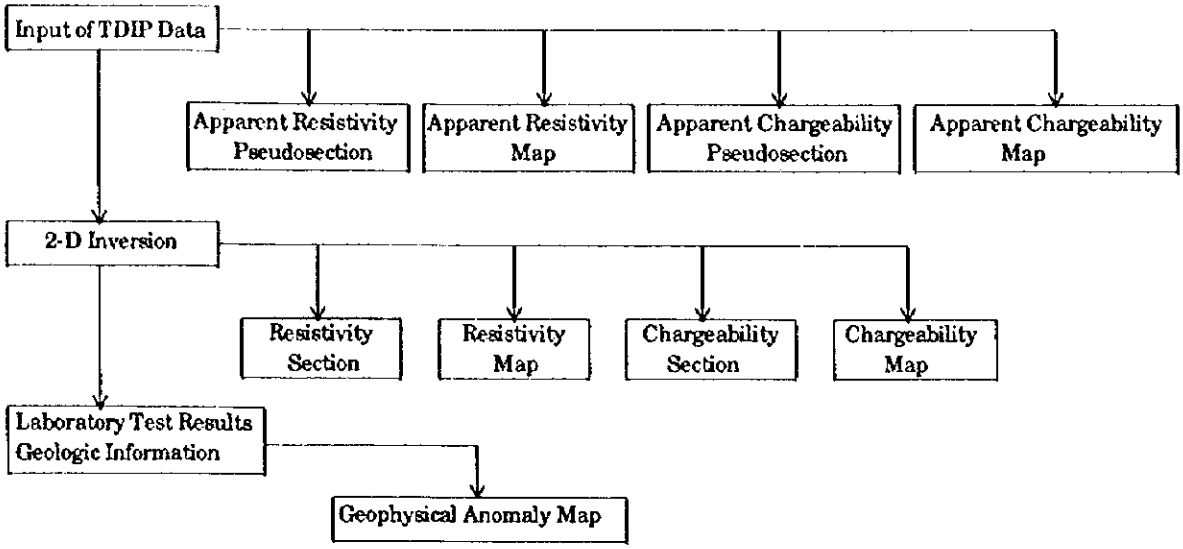

Fig. 2-4-3 Flow Chart of the Analytical Method

(1) Apparent Resistivity Pseudosection

In this section, apparent resistivity is plotted at the depth of "a(n+1)/2" just under the middle point of the used electrodes for each line. In the above equation, "a" is electrode spacing and "n" is electrode separation index.

(2) Apparent Resistivity Map

In this map, the apparent resistivity of the specific electrode separation index is plotted.

(3) Apparent Chargeability Pseudosection

In this section, apparent chargeability is plotted at the depth of "a(n+1)/2" just under the middle point of the used electrodes for each line. In the above equation, "a" is electrode spacing and "n" is electrode separation index.

(4) Apparent Chargeability Map

In this map, the apparent chargeability of the specific electrode separation index is plotted.

(5) 2-D Inversion

This analysis assumes that structure is two dimensional, and determines the optimum resistivity

distribution of two dimensional model for each line. The distribution of apparent resistivity calculated for the optimum model is best matched to that of the observed apparent resistivity. The finite element method is applied to the forward analysis and the non-linear least squares method with smoothness constraint is applied to the optimization of resistivity distribution.

After resistivity distribution is obtained, chargeability distribution is determined with the least squares method on the assumption that an observed chargeability is weighted average value of chargeability using the sensitivities of apparent resistivity as a weighting function.

(6) Resistivity Section

In this section, the resistivity distribution below each line is drawn using the results of the 2-D inversion.

(7) Resistivity Map

In this map, the resistivity distribution at the specific level is drawn using the results of the 2-D inversion.

(8) Chargeability Section

In this section, the chargeability distribution below each line is drawn using the results of the 2-D inversion.

(9) Chargeability Map

In this map, the chargeability distribution at the specific level is drawn using the results of the 2-D inversion.

(10) Geophysical Anomaly Map

In this map, the geophysical anomalies are extracted.

4-3 Survey Results

4-3-1 Observed data

(1) Apparent Resistivity

The pseudosections of the apparent resistivity of every line are shown in Figures 2-4-4 to 2-4-9 and the maps of the apparent resistivity of n=2 and 4 are shown in Figures 2-4-10 and 2-4-11. The resistivity in this area is high on the whole, since the mean value of apparent resistivity is about 600 ohm-m. Resistivity is clearly higher in the deeper zone. Low resistivity areas less than 100 ohm-m are distributed in the shallow and flat zones. Roughly speaking, the resistivity of the south of line K is higher than that of the north of line J.

(2) Apparent Chargeability

The pseudosections of the apparent chargeability of every line are shown in Figures 2-4-12 to 2-4-17 and the maps of the apparent chargeability of n=2 and 4 are shown in Figures 2-4-18 and 2-4-19. The background value of chargeability in this area seems to be 3－5 mV/V, judging from the apparent chargeability. The chargeability anomaly zones exceeding 10 mV/V were detected around stations G-22 to J-15 (NW-SE direction) in the shallow zone, and in addition, around stations B-10 to B-15, stations K-27 to Q-18 (N-S direction) and stations L-14 to O-12 (N-S direction) in the deeper zone.

4-3-2 Analytic results (2-D Inversion)

(1) Resistivity

The resistivity sections drawn with the 2-D inversion are shown in Figures 2-4-20 to 2-4-25. The resistivity maps of 2 levels (SL 900 m and SL 800 m) are shown in Figures 2-4-26 and 2-4-27. The 2-D inversion led to the clear distribution and contrast of the resistivity in this area. The high resistivity zones more than 1,000 ohm-m are distributed throughout the survey area, except in the shallow zone. The low resistivity zones of less than 100 ohm-m in the shallow zone are distributed in the flat parts and have the largest thickness of about 50m. In the map of SL 900m (the depth of about 50m below the surface), relatively lower resistivity zones correspond to the flat parts, as a whole. In the map of SL 800m (the depth of about 150m below the surface), the high resistivity zones of more than 1,000 ohm-m are distributed in almost all of the survey area. While, low resistivity areas in the deeper zone were detected at station B-1, station B-8, station H-22, station J-22, station J-14 and station Q-35.

(2) Chargeability

The chargeability sections drawn with the 2-D inversion are shown in Figures 2-4-28 to 2-4-33. The chargeability maps of 2 levels (SL 900 m and SL 800 m) are shown in Figures 2-4-34 to 2-4-35. By the 2-D inversion, chargeability anomalies were extracted clearly. In the shallow zone, the background value covers, except for the weak chargeability anomaly detected in the vicinity of the North Prospect on lines G to I. In the deeper level of SL 800m, the strong chargeability anomalies of more than 24 mV/V were extracted in the three zones around station B-12, station J-25 and station M-27.

The anomaly zone around station B-12 exceeding 50 mV/V is the strongest in this area and tends to extend to line A. The anomaly zone around station J-25 has a NW-SE direction and continues to line K. The anomaly zone around station M-27 exhibits a N-S direction and tends to continue up to line P. All of these anomaly zones show vertical structure.

All of the strong chargeability anomalies in the deeper zone are distributed in high resistivity zones of more than 1,000 ohm-m. On the other hand, the weak chargeability anomalies in the shallow zone are distributed in relatively low resistivity zone of several hundred ohm-m.

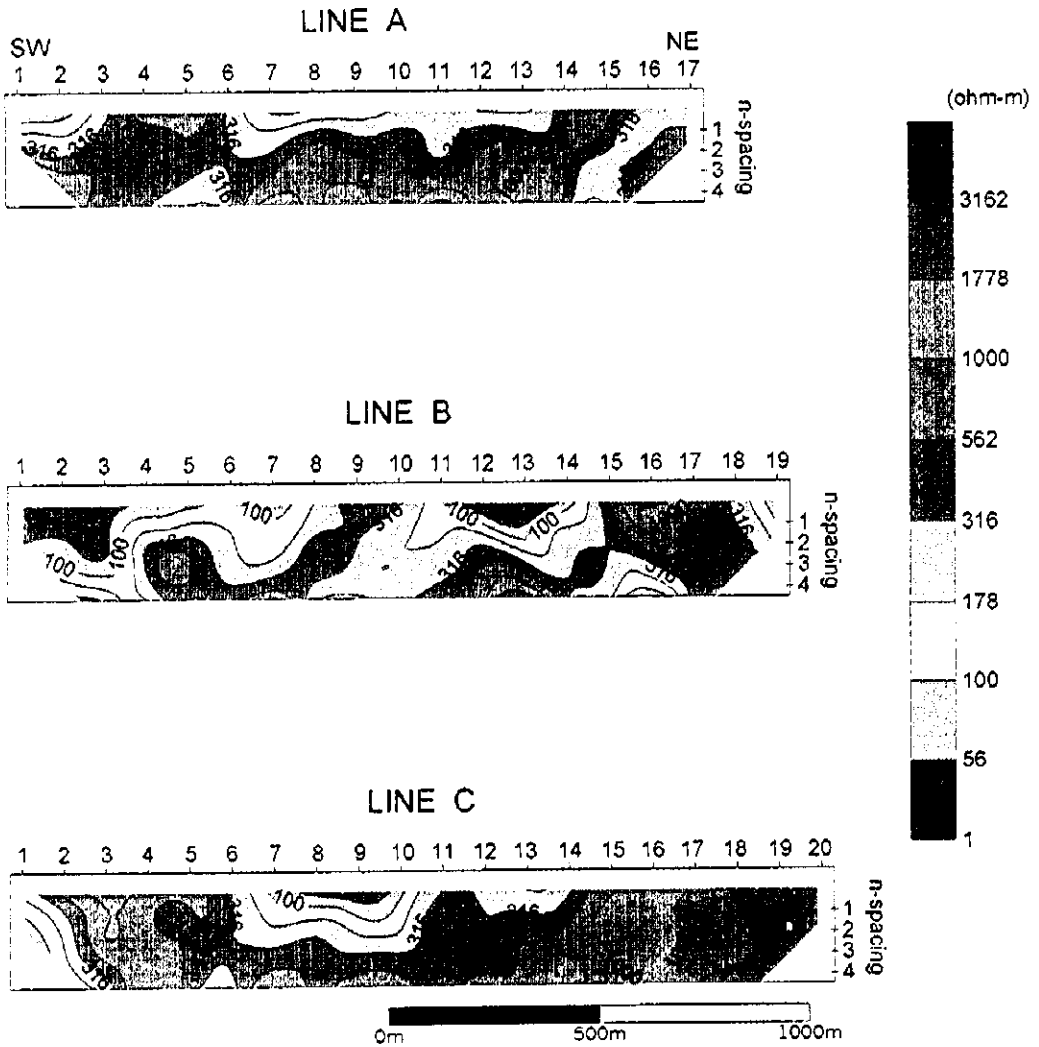

Fig. 2-4-4 Apparent Resistivity Pseudosection (Line A, B, C)

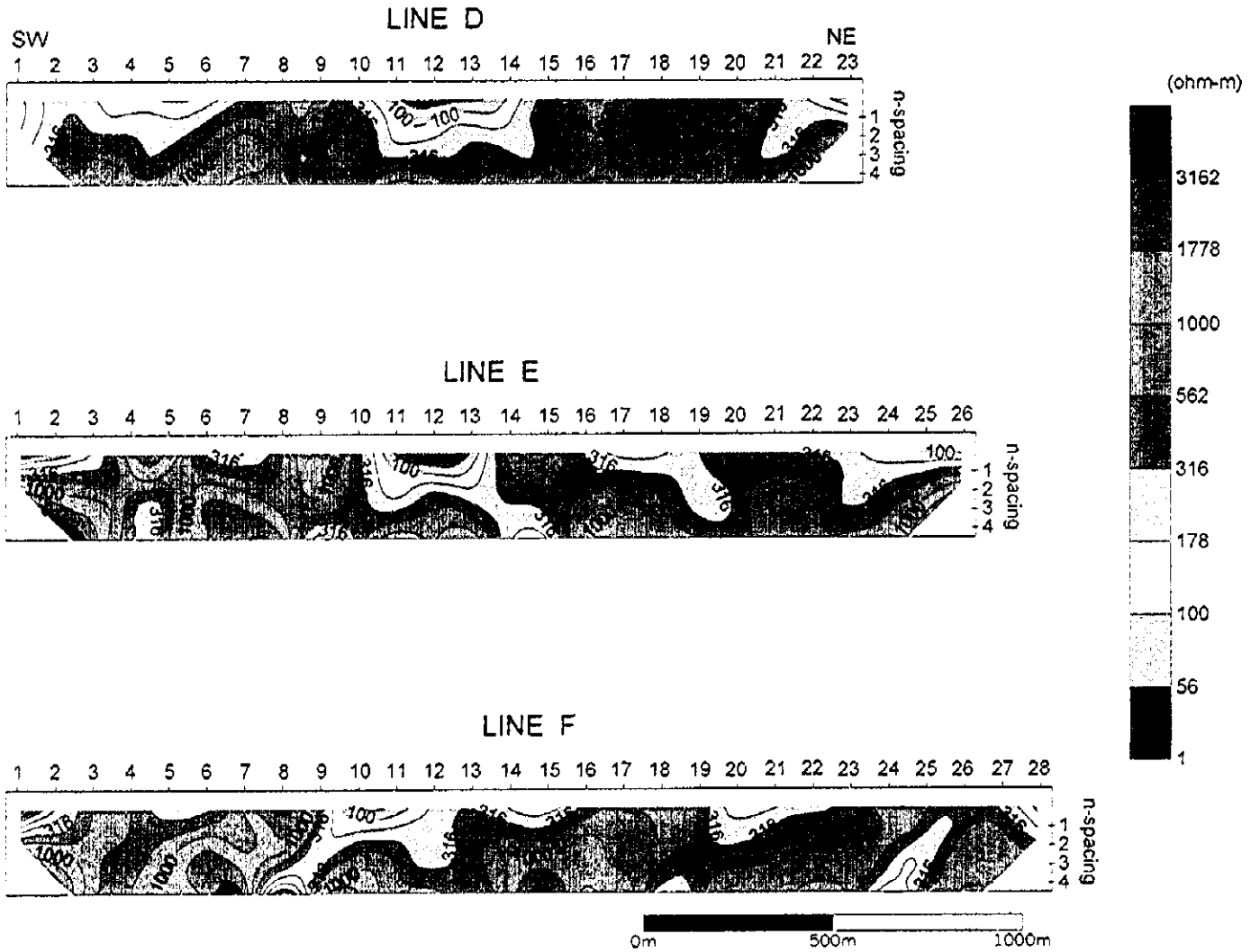

Fig. 2-4-5 Apparent Resistivity Pseudosection (Line D, E, F)

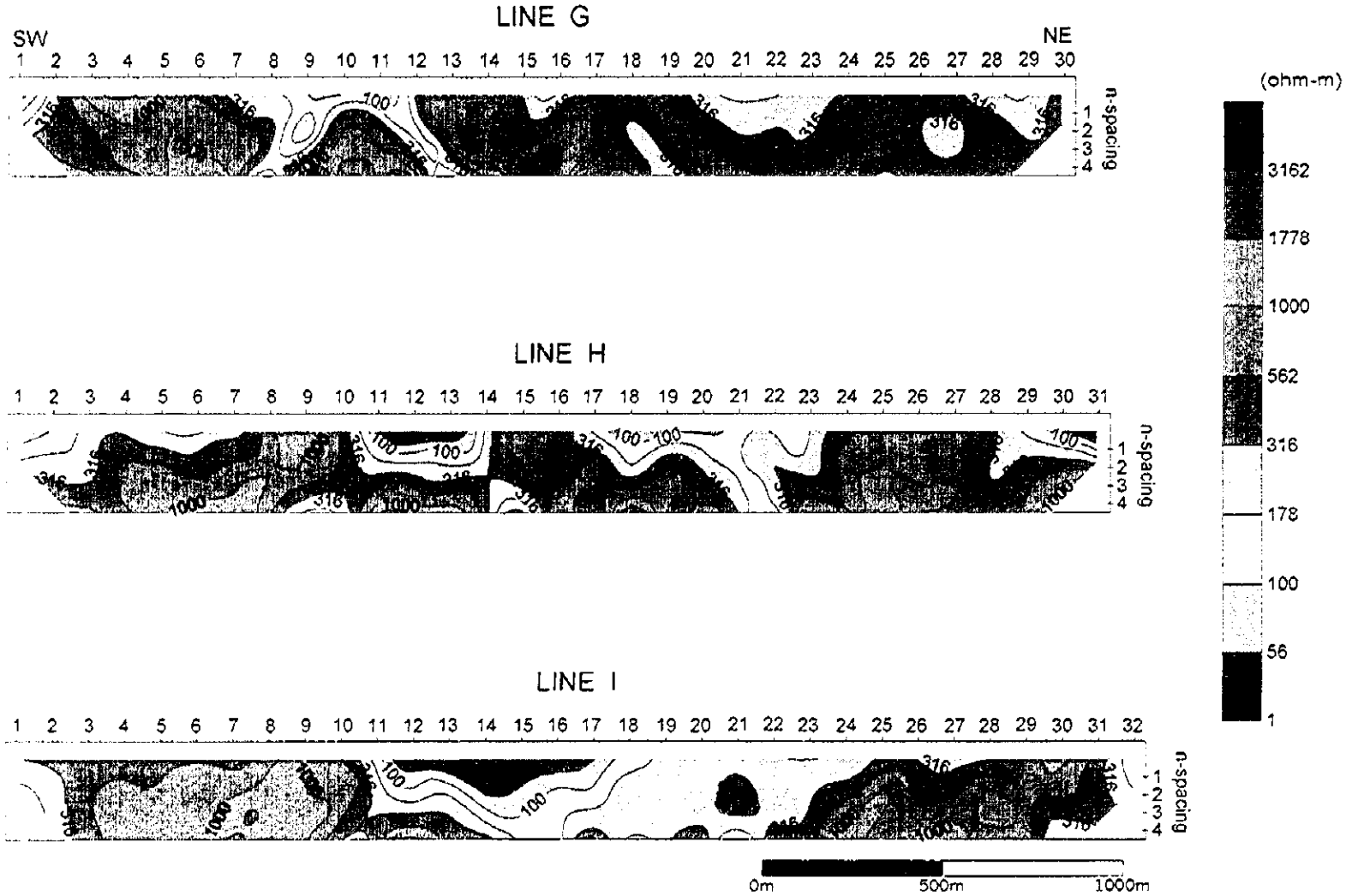

Fig. 2-4-6 Apparent Resistivity Pseudosection (Line G, H, I)

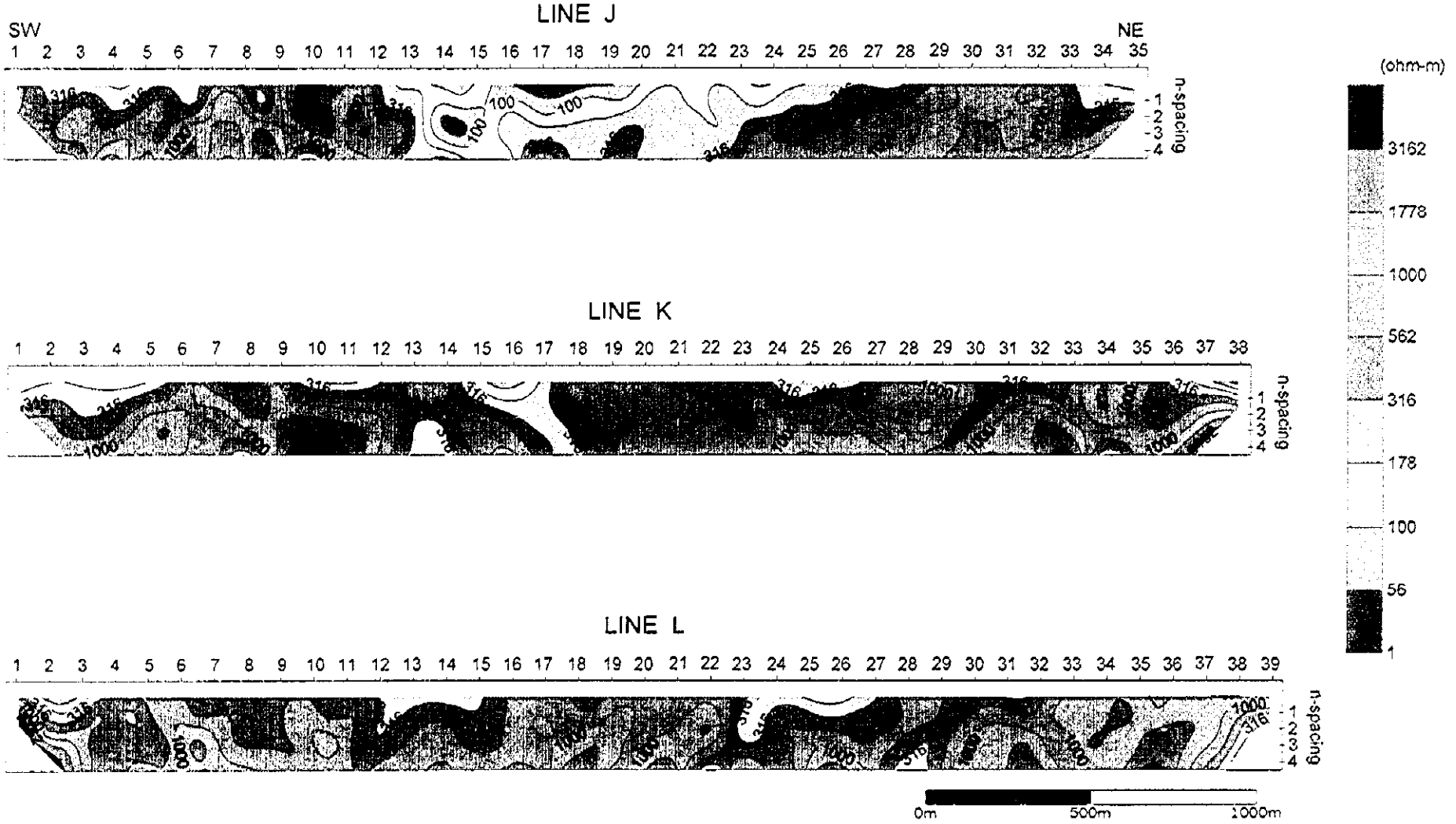

Fig. 2-4-7 Apparent Resistivity Pseudosection (Line J, K, L)

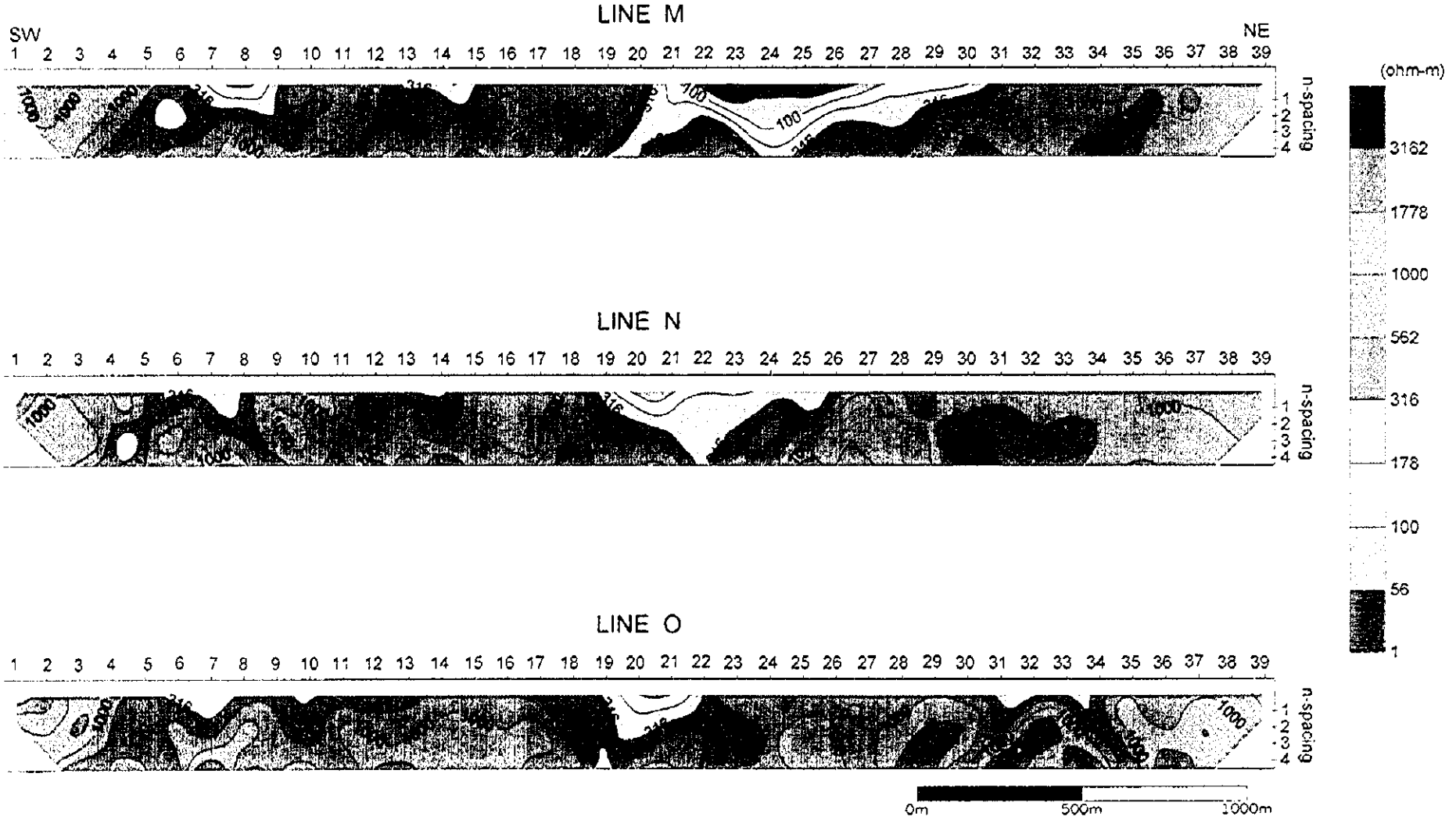

Fig. 2-4-8 Apparent Resistivity Pseudosection (Line M, N, O)

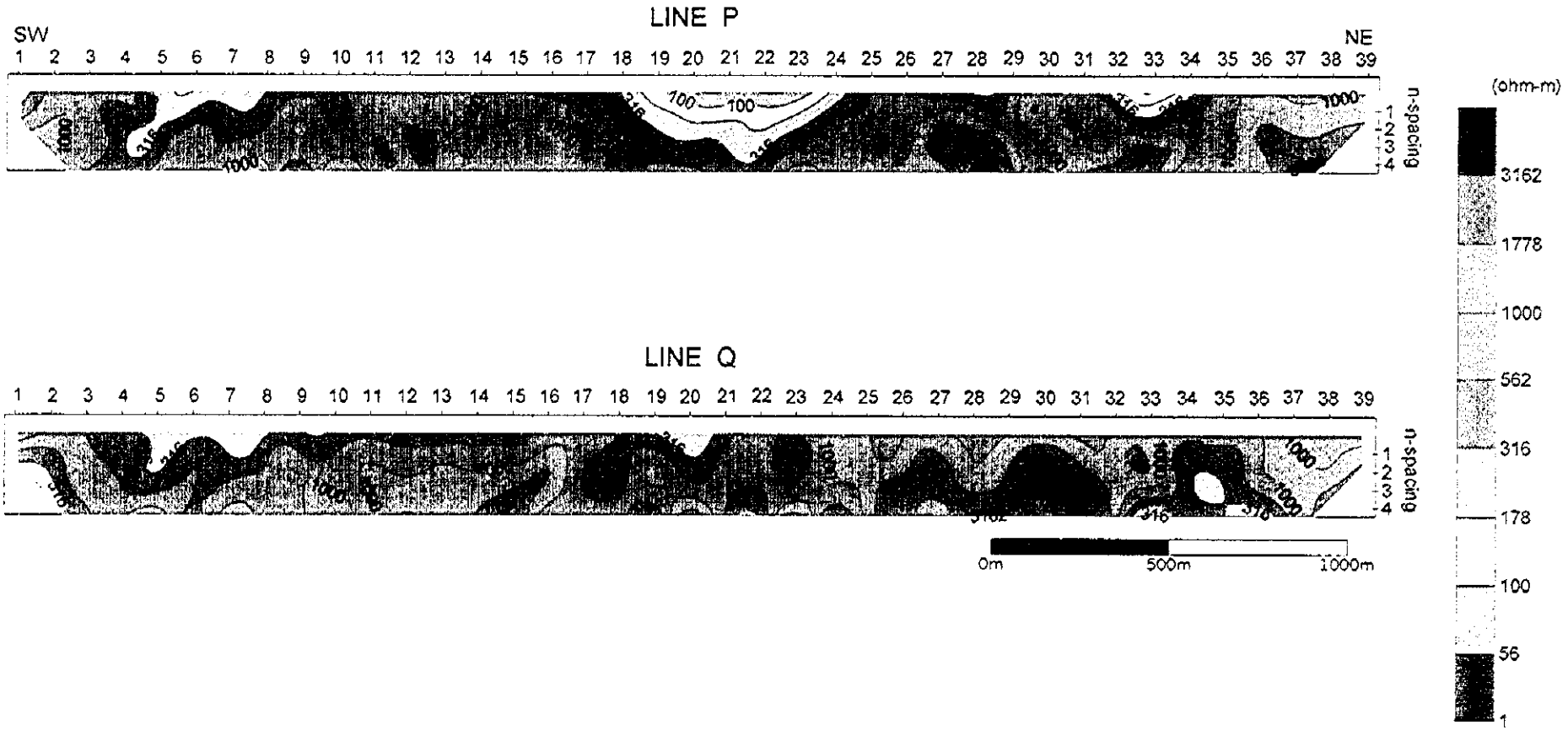

Fig. 2-4-9 Apparent Resistivity Pseudosection (Line P, Q)

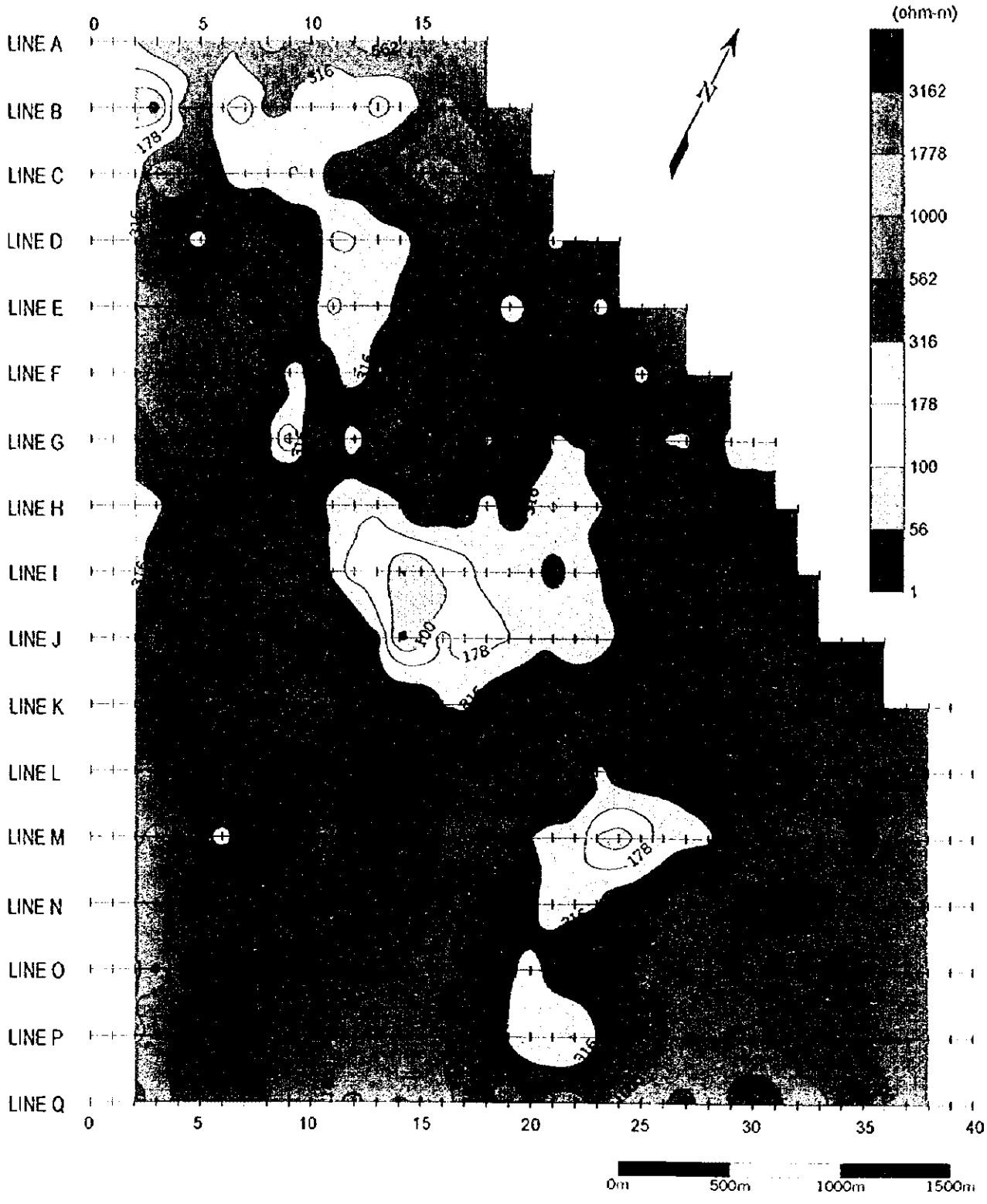

Fig. 2-4-10 Apparent Resistivity Map (n=2)

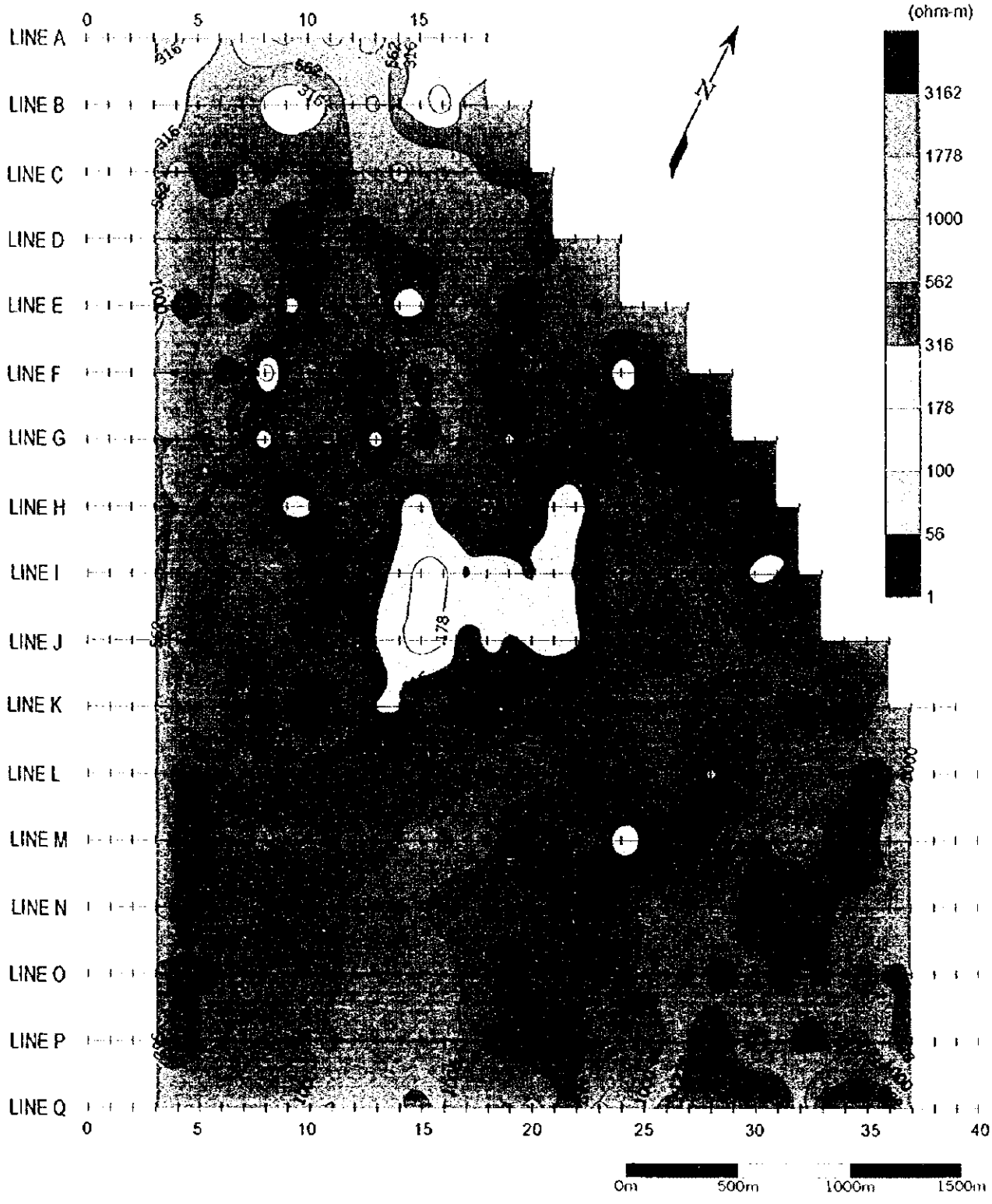

Fig. 2-4-11 Apparent Resistivity Map (n=4)

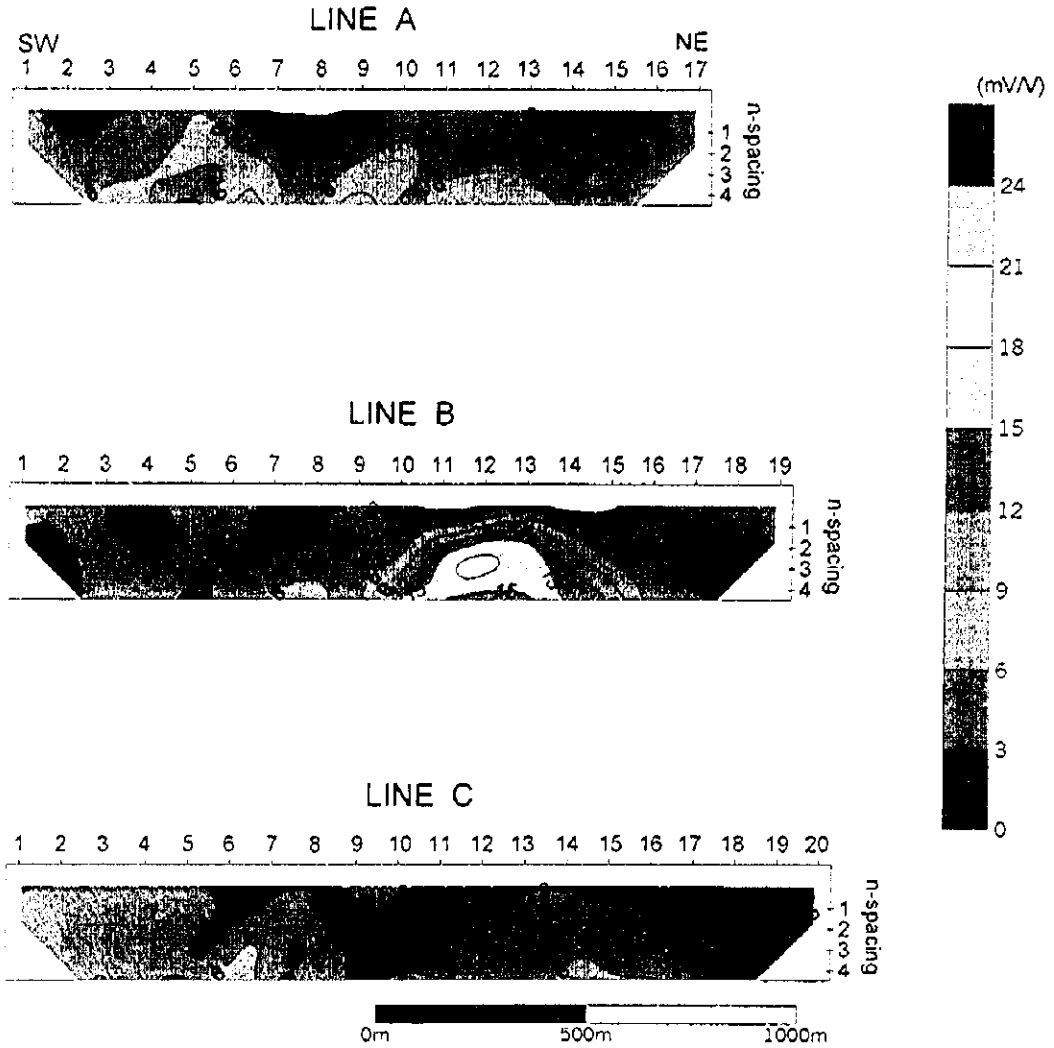

Fig. 2-4-12 Apparent Chargeability Pseudosection (Line A, B, C)

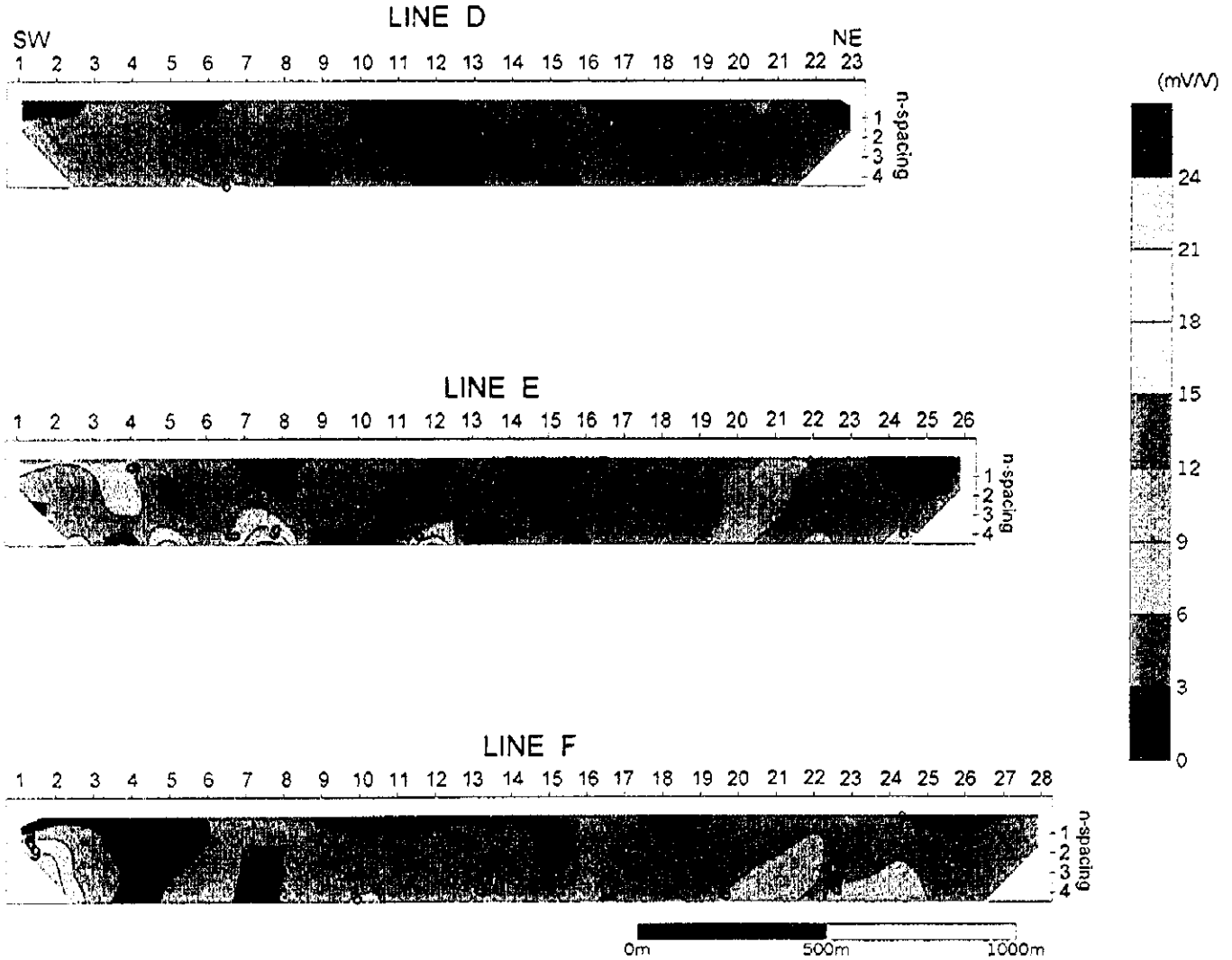

Fig. 2-4-13 Apparent Chargeability Pseudosection (Line D, E, F)

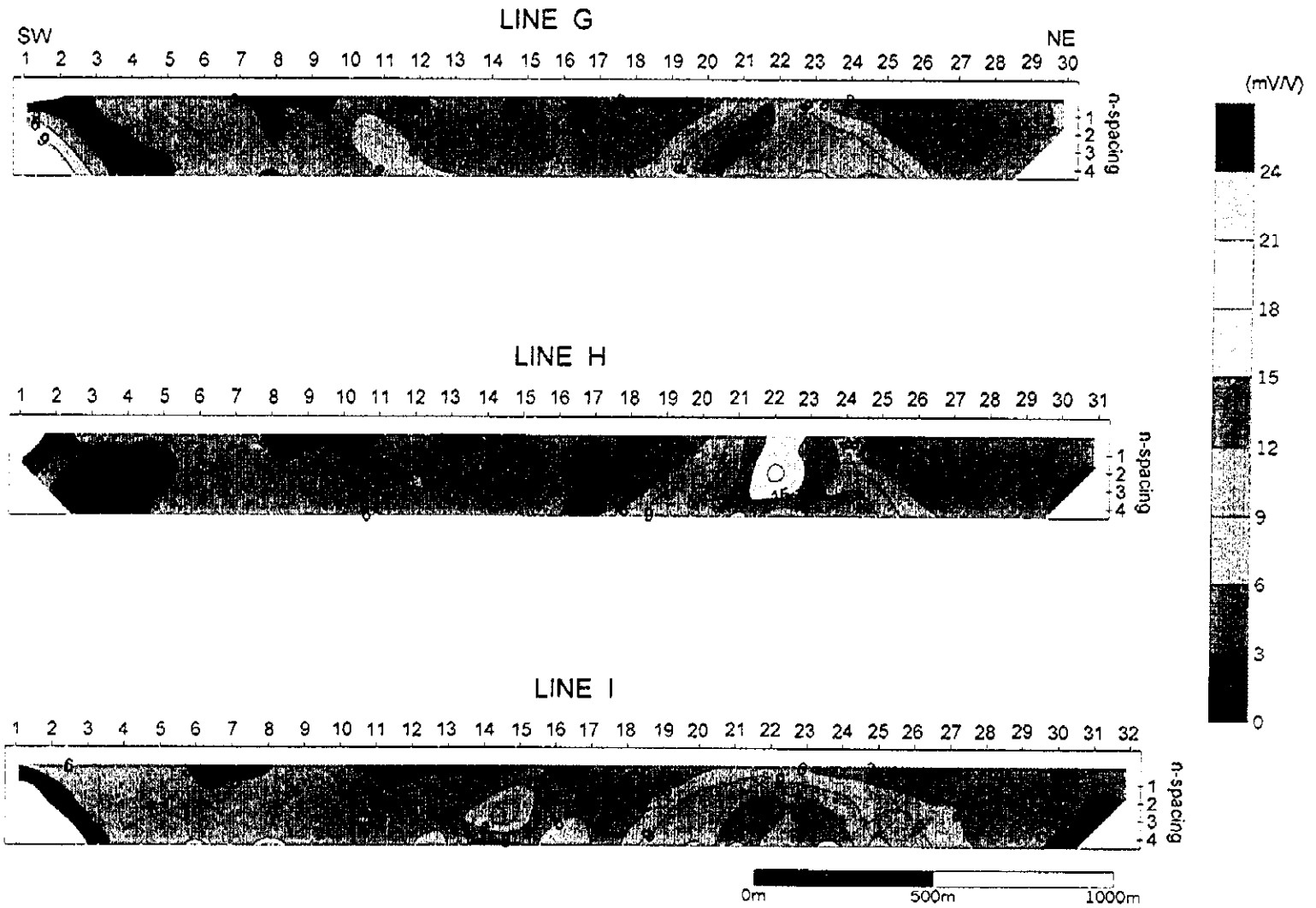

Fig. 2-4-14 Apparent Chargeability Pseudosection (Line G, H, I)

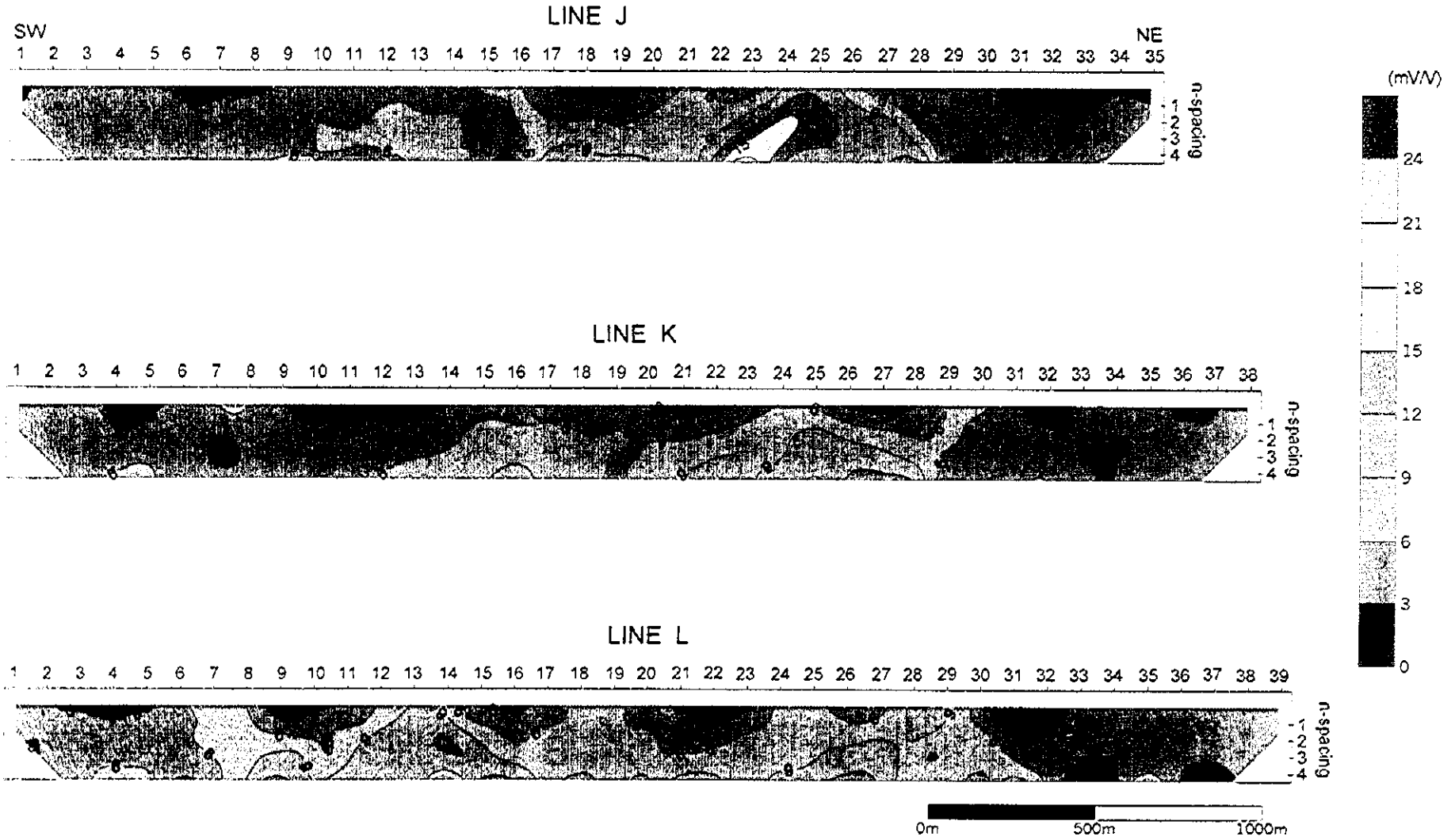

Fig. 2-4-15 Apparent Chargeability Pseudosection (Line J, K, L)

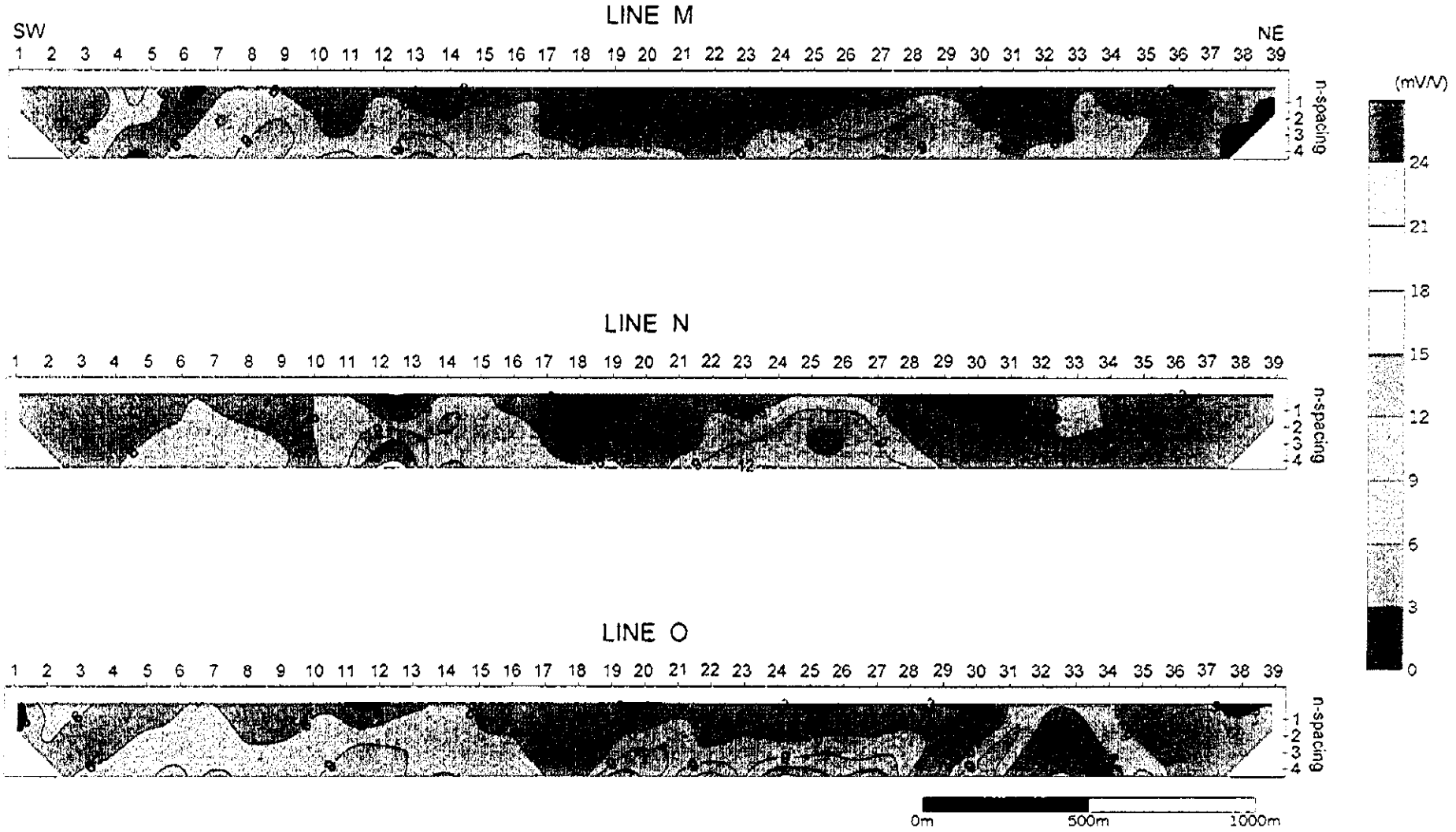

Fig. 2-4-16 Apparent Chargeability Pseudosection (Line M, N, O)

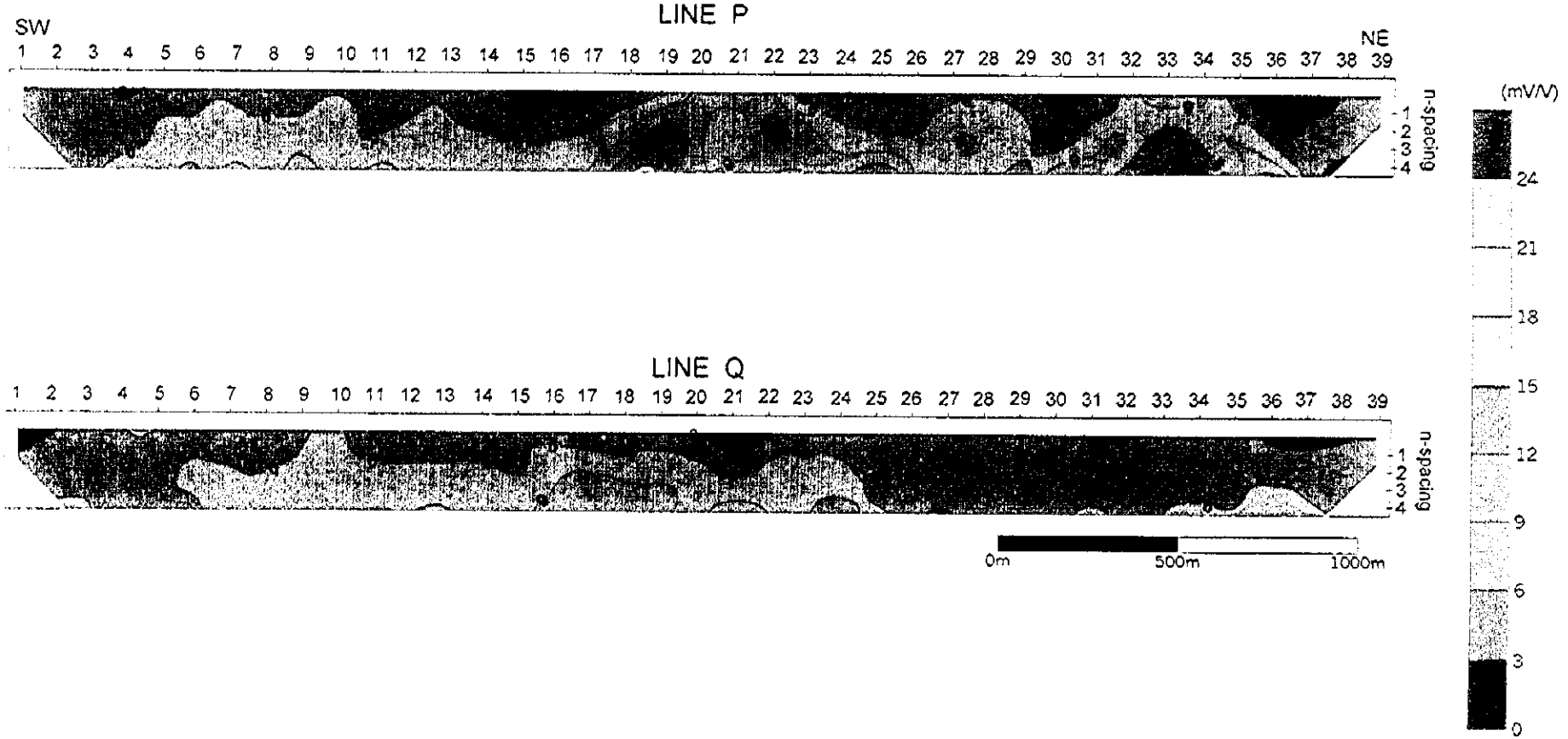

Fig. 2-4-17 Apparent Chargeability Pseudosection (Line P, Q)

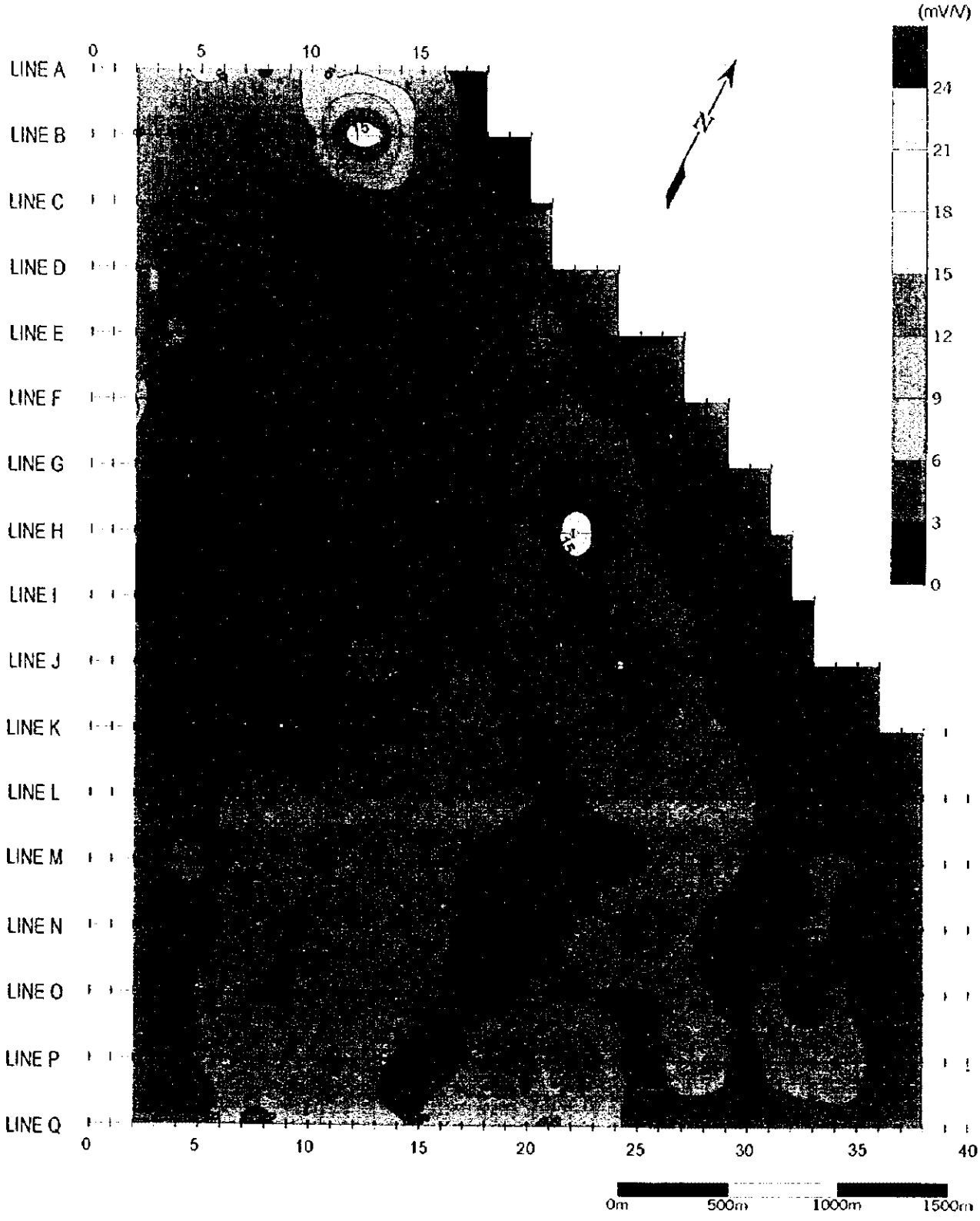

Fig. 2-4-18 Apparent Chargeability Map (n=2)

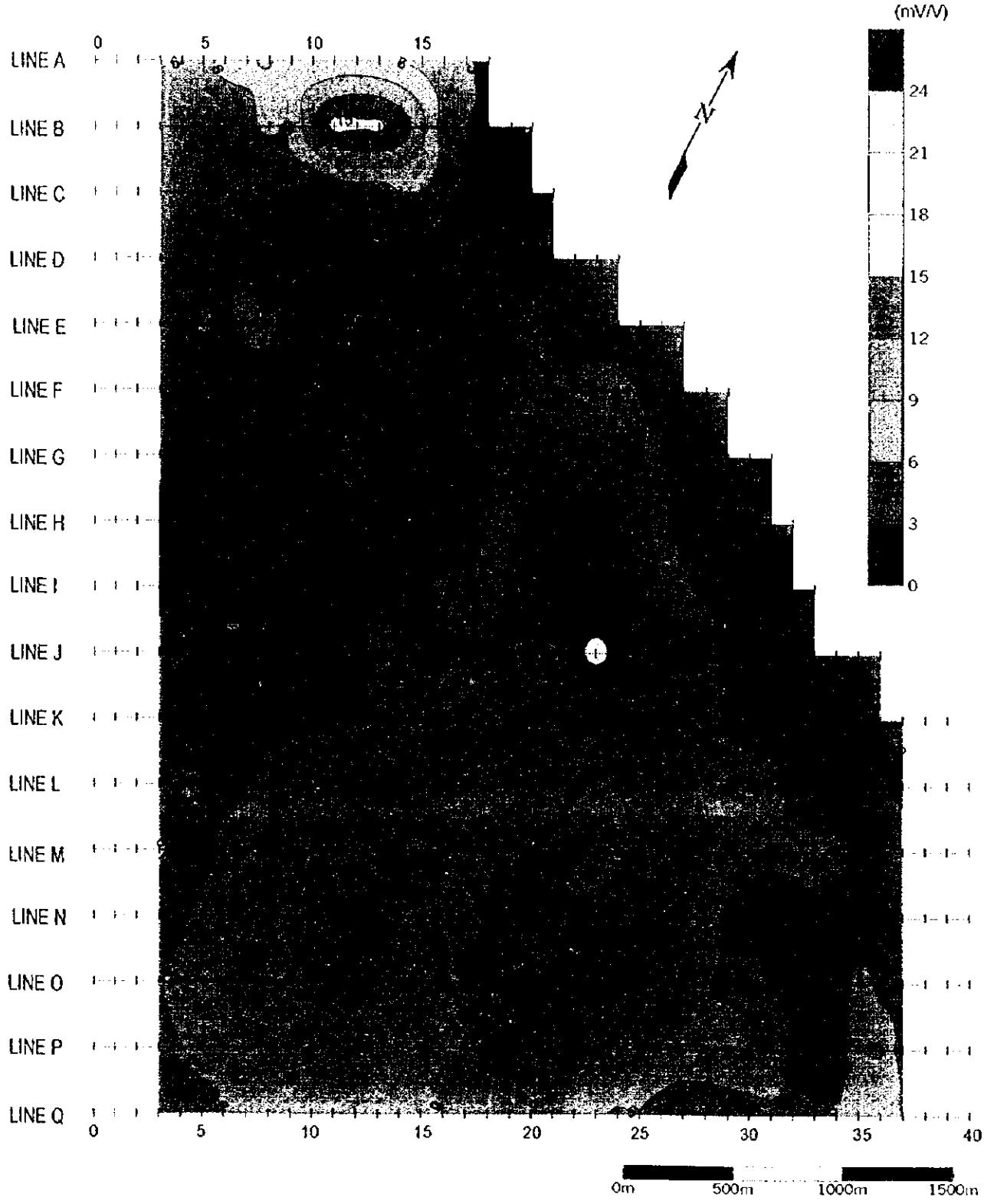

Fig. 2-4-19 Apparent Chargeability Map (n=4)

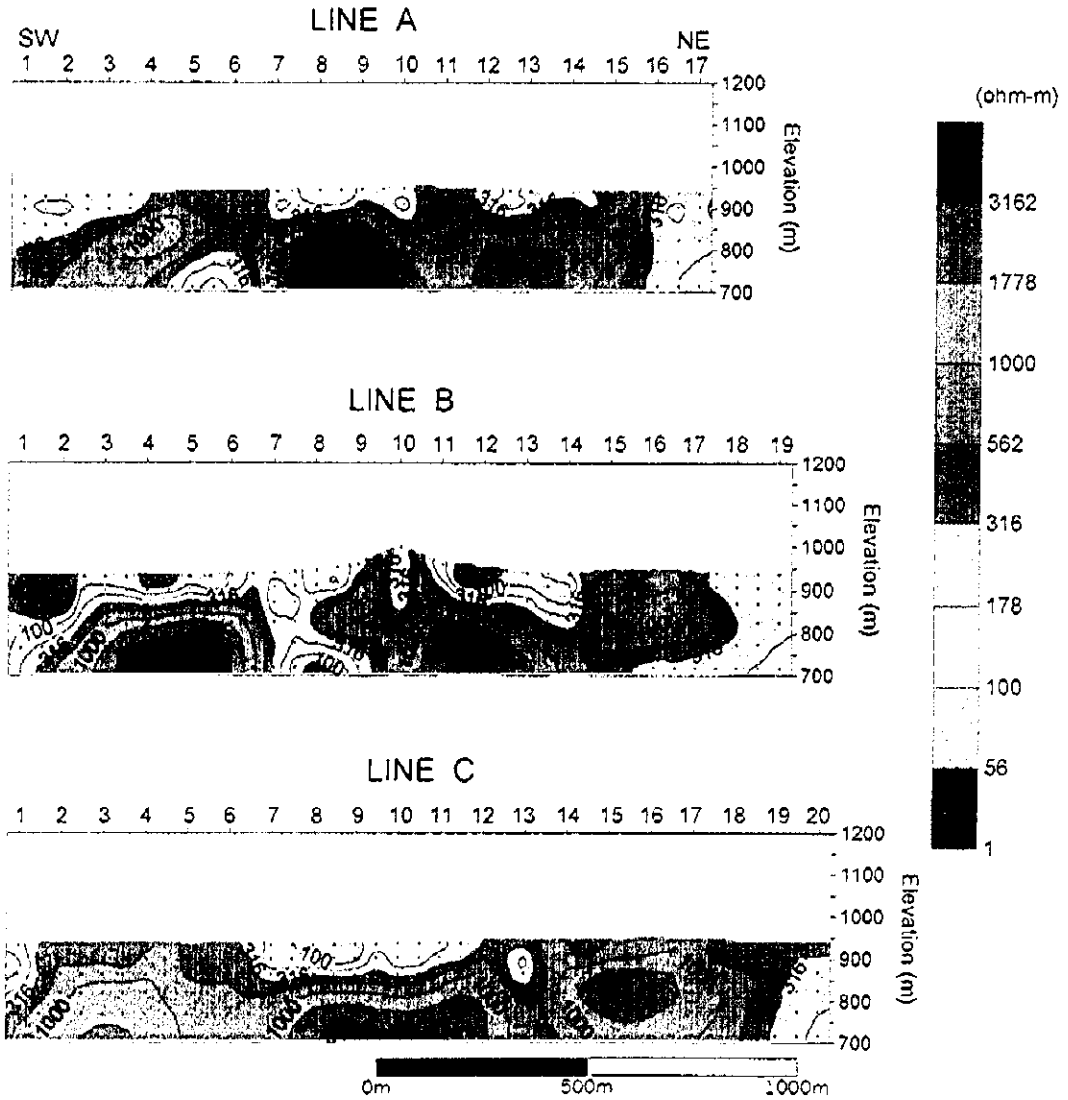

Fig. 2-4-20 Resistivity Section (A, B, C)

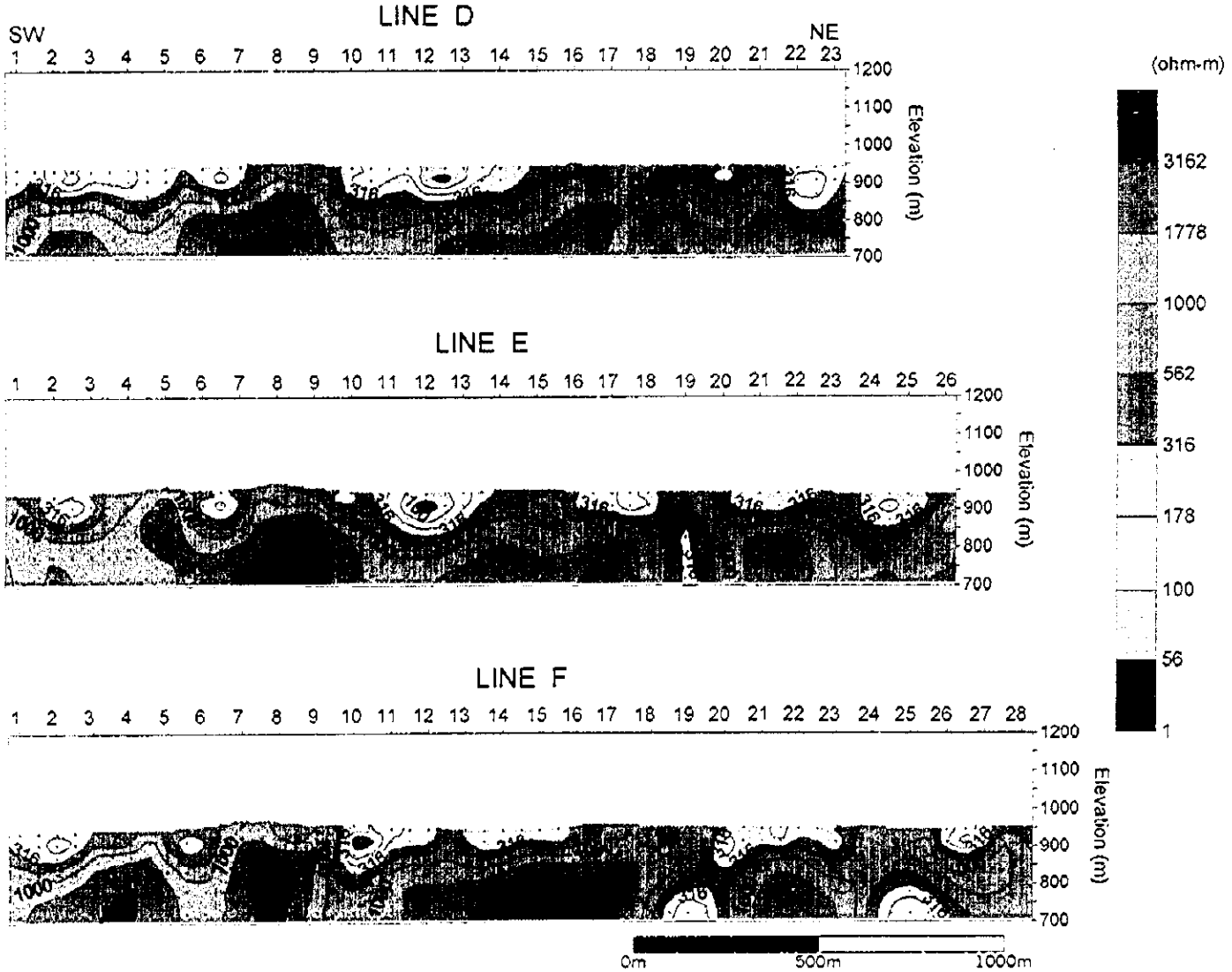

Fig. 2-4-21 Resistivity Section (D, E, F)

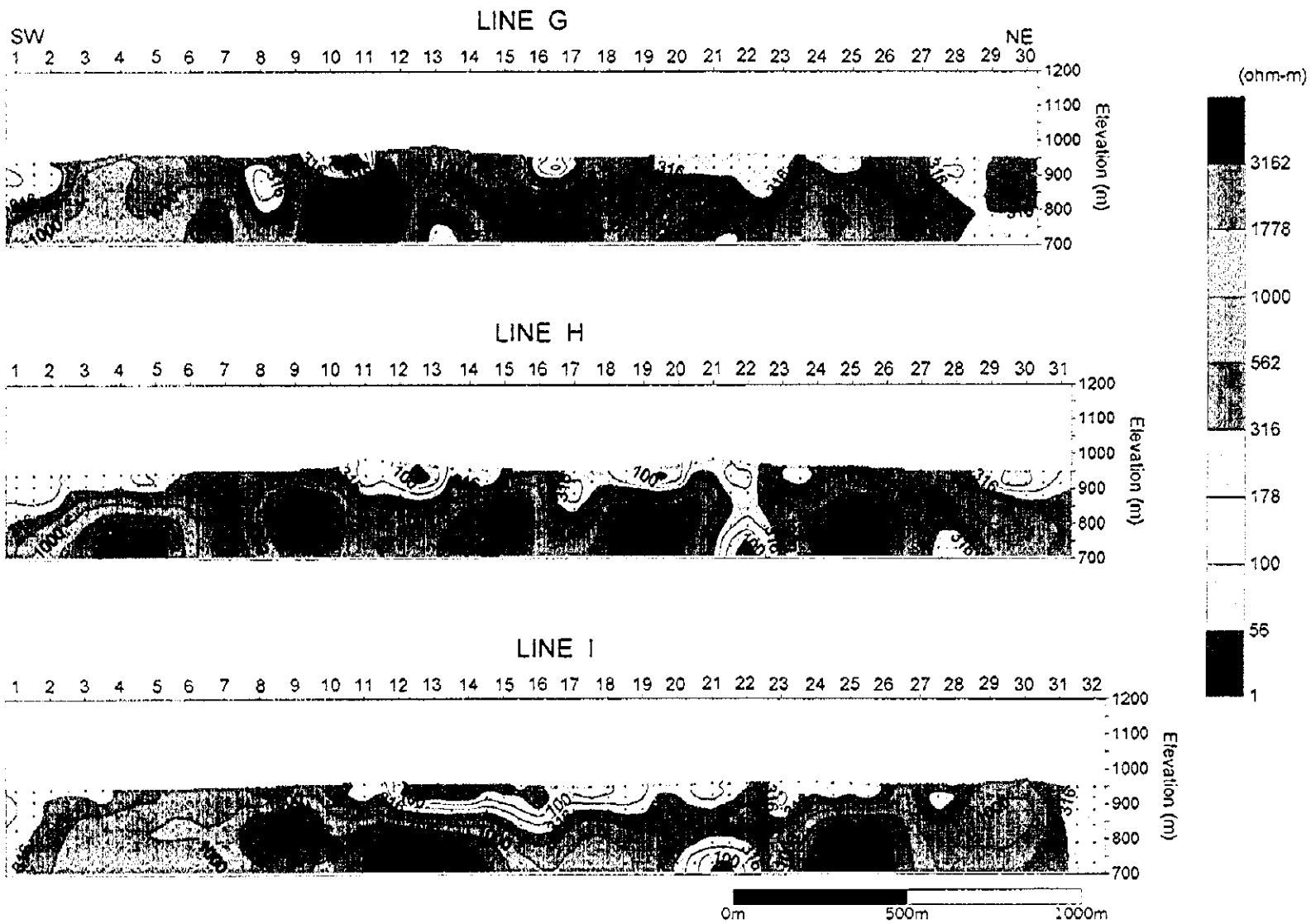

Fig. 2-4-22 Resistivity Section (G, H, I)

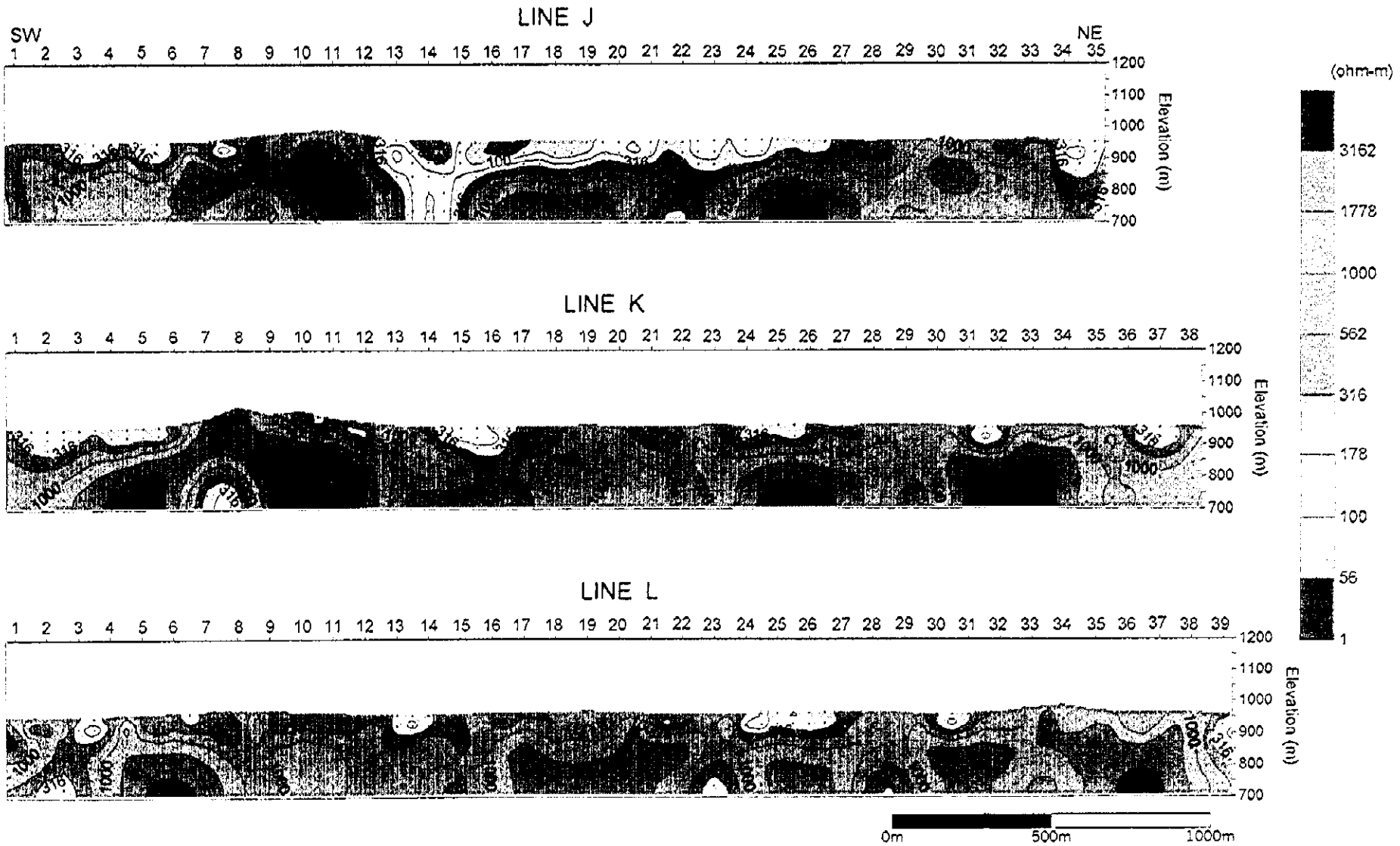

Fig. 2-4-23 Resistivity Section (J, K, L)

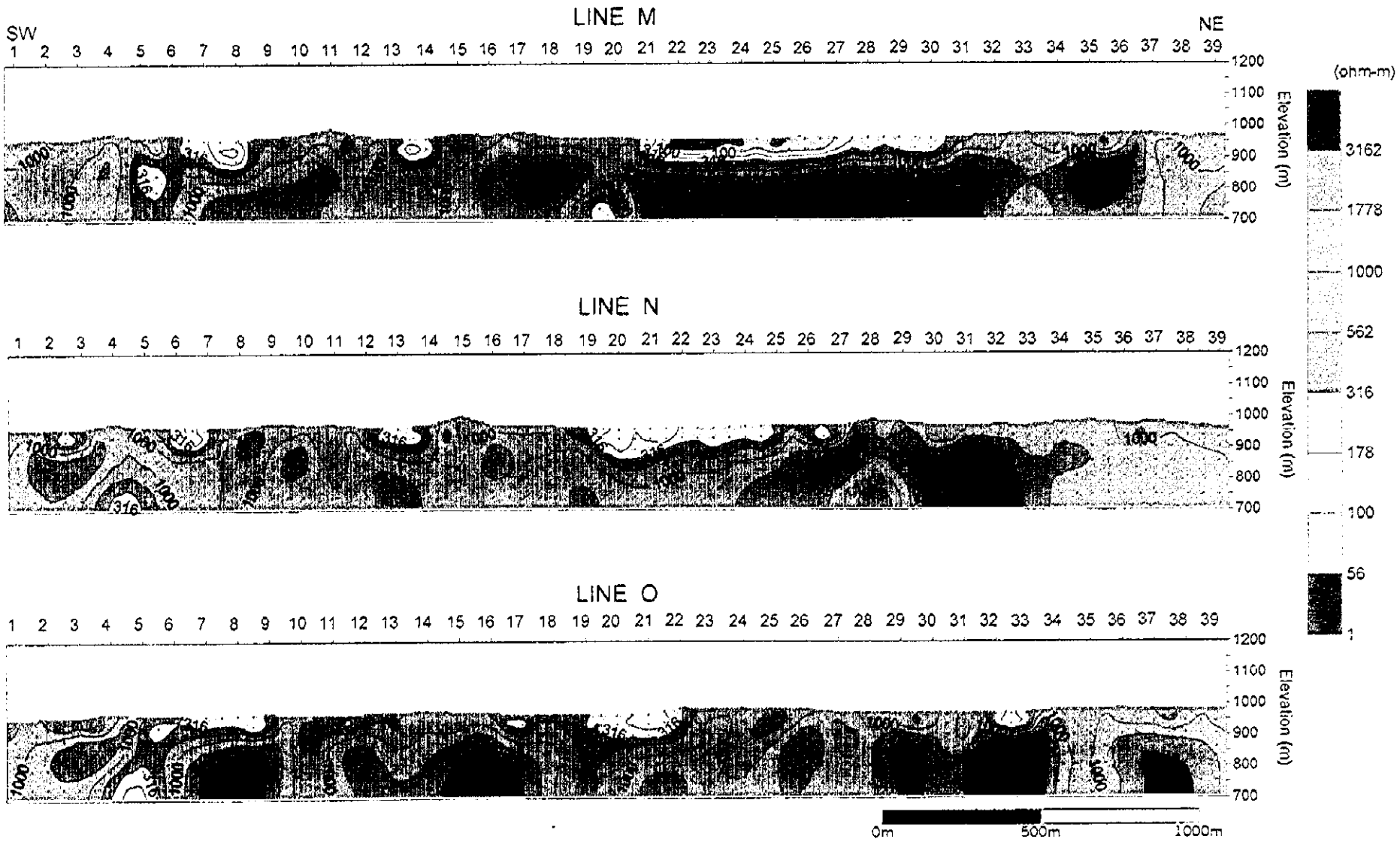

Fig. 2-4-24 Resistivity Section (M, N, O)

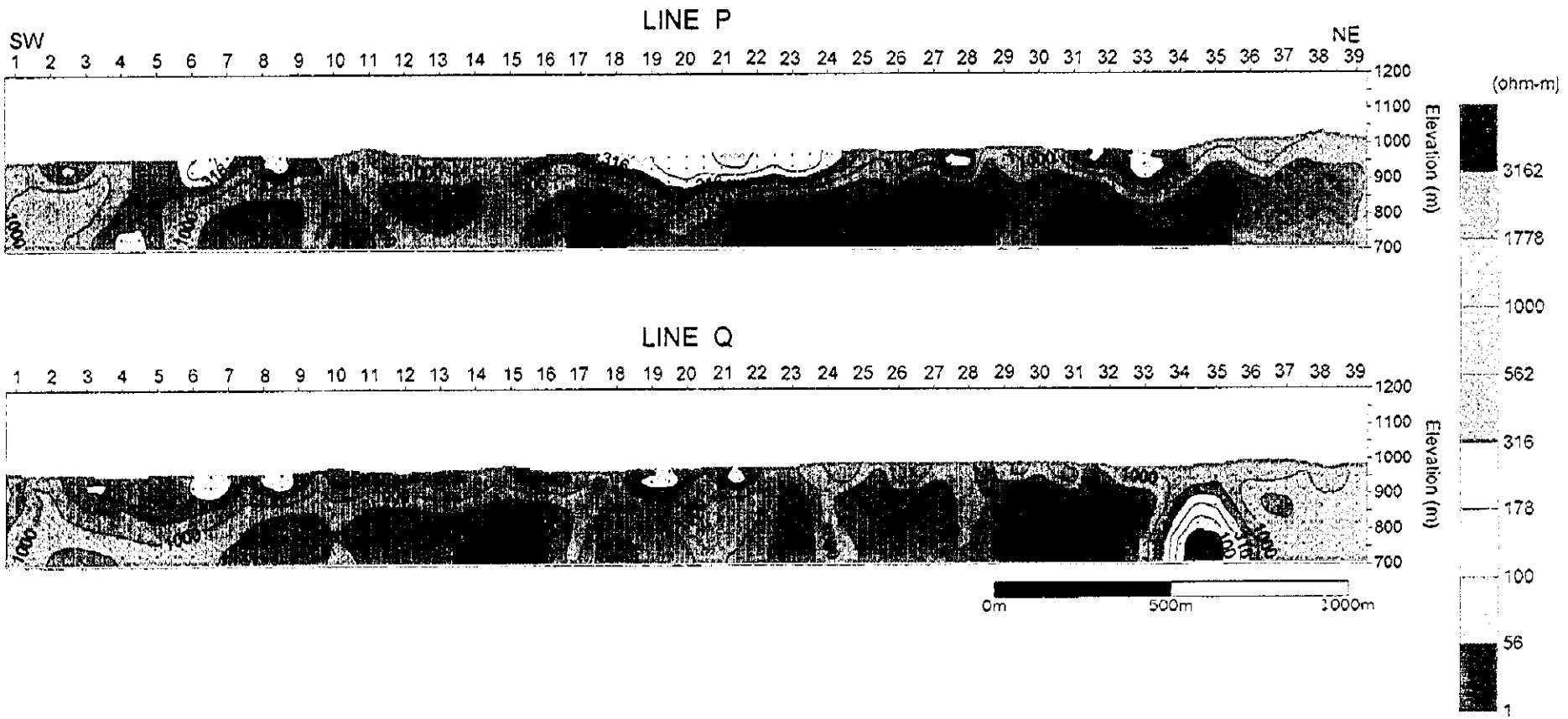

Fig. 2-4-25 Resistivity Section (P, Q)

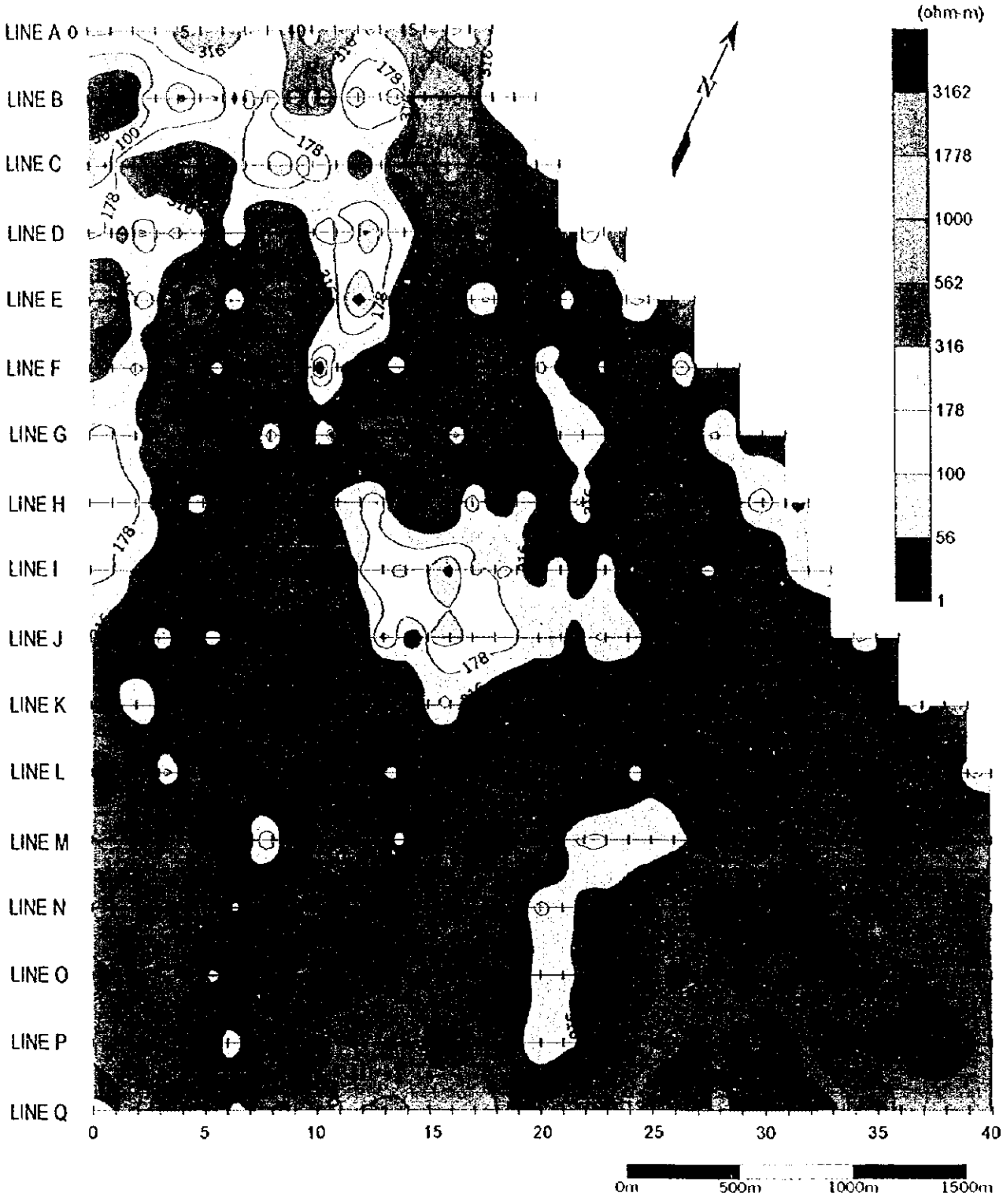

Fig. 2-4-26 Resistivity Map (SL 900m)

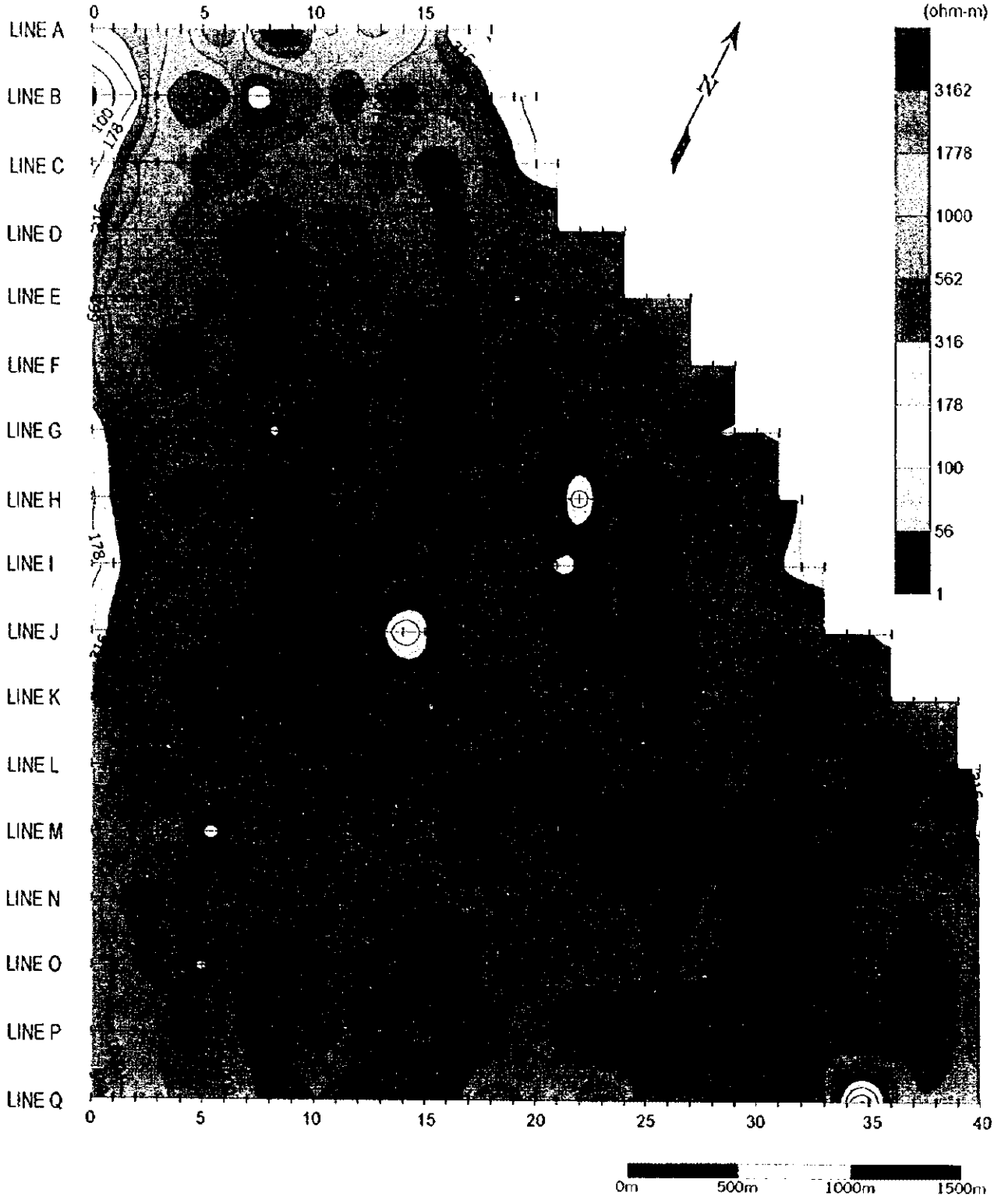

Fig. 2-4-27 Resistivity Map (SL 800m)

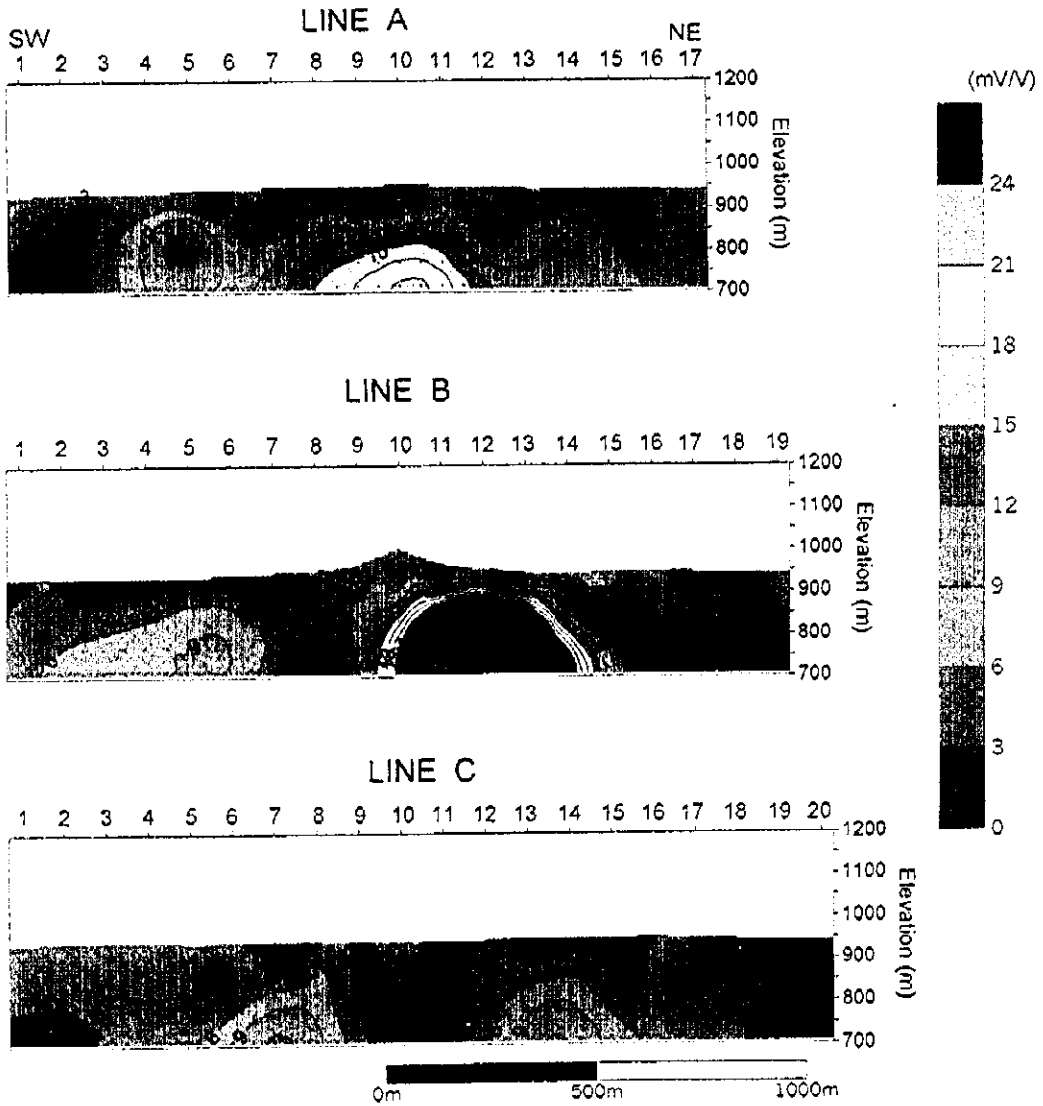

Fig. 2-4-28 Chargeability Section (A, B, C)

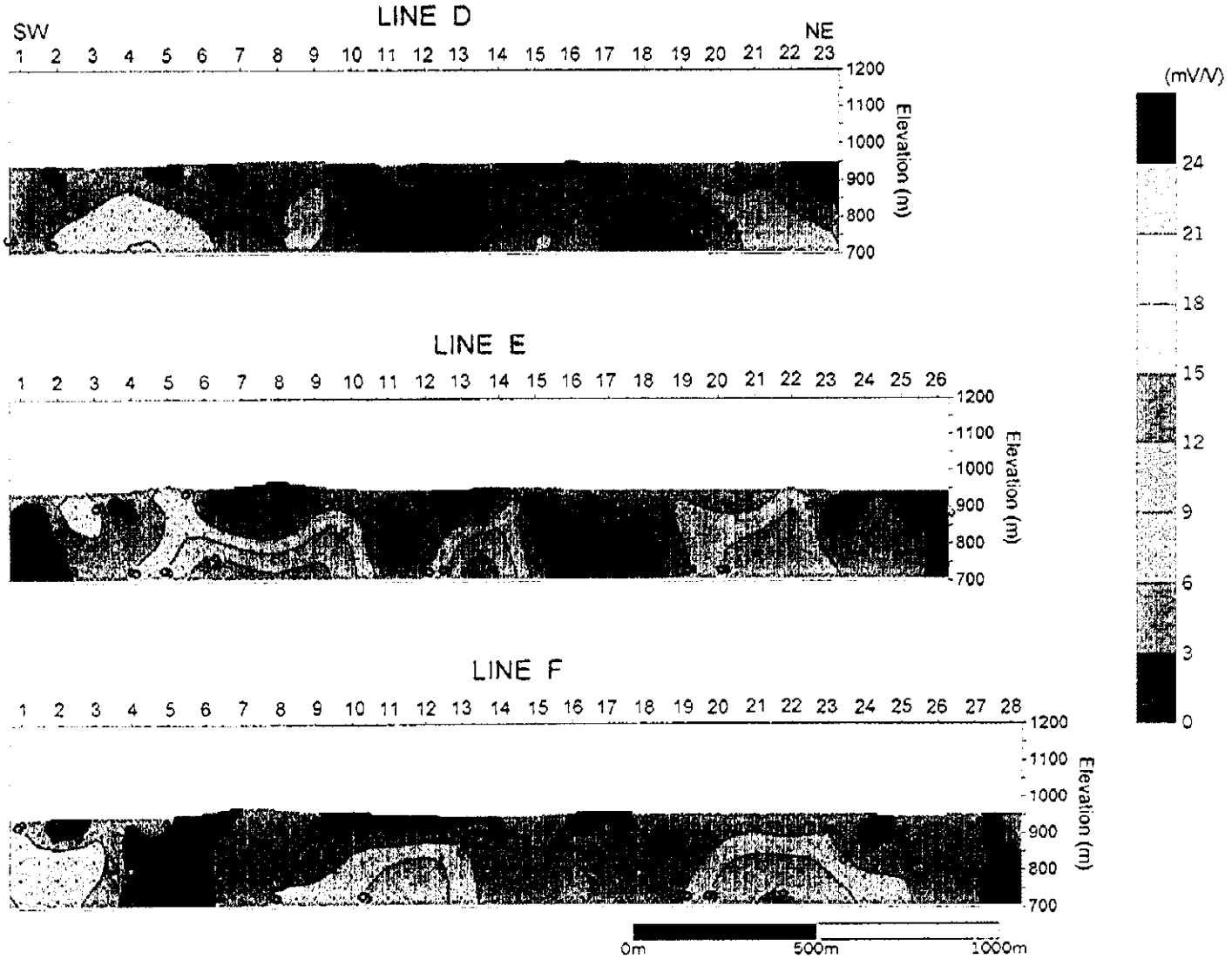

Fig. 2-4-29 Chargeability Section (D, E, F)

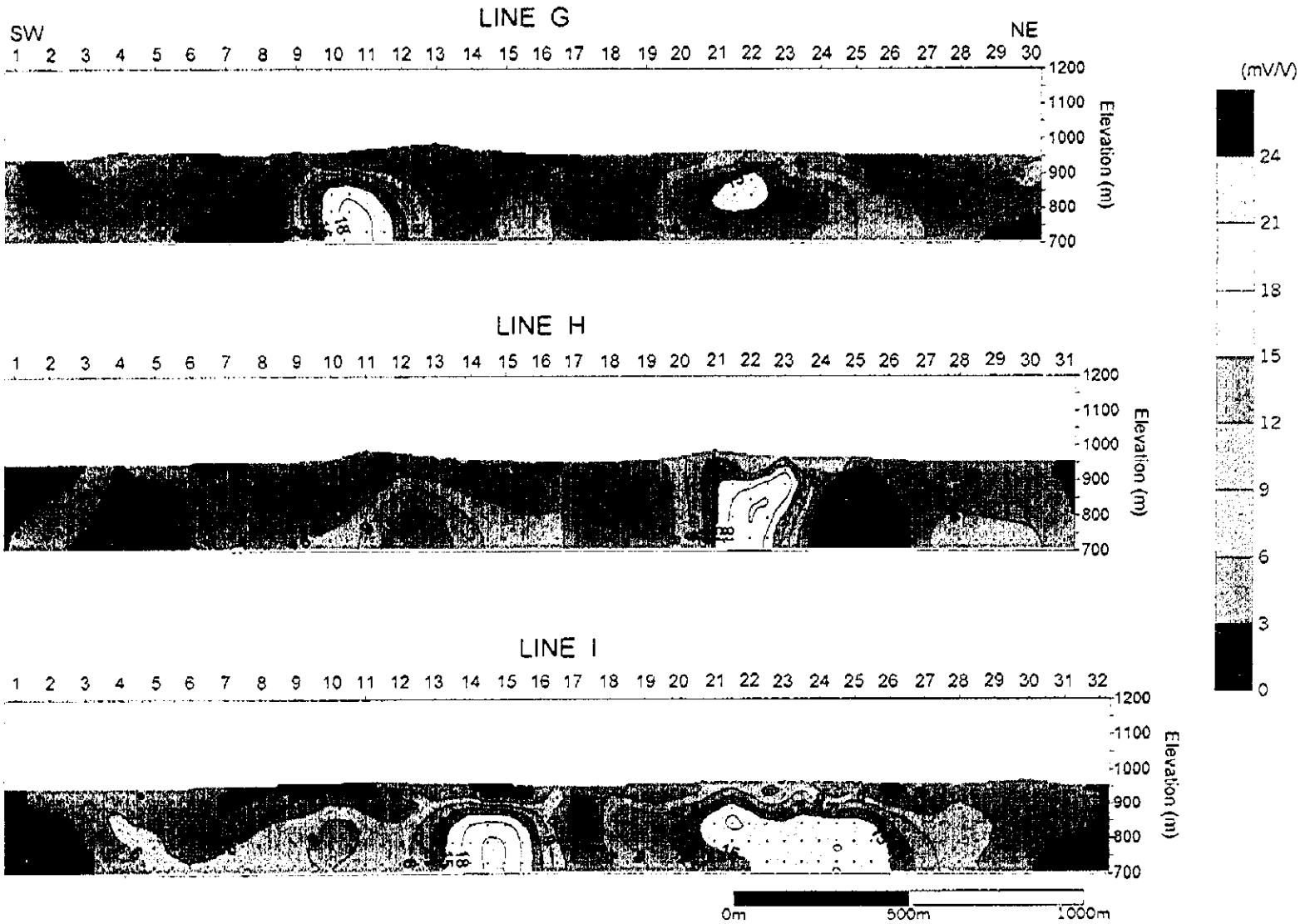

Fig. 2-4-30 Chargeability Section (G, H, I)

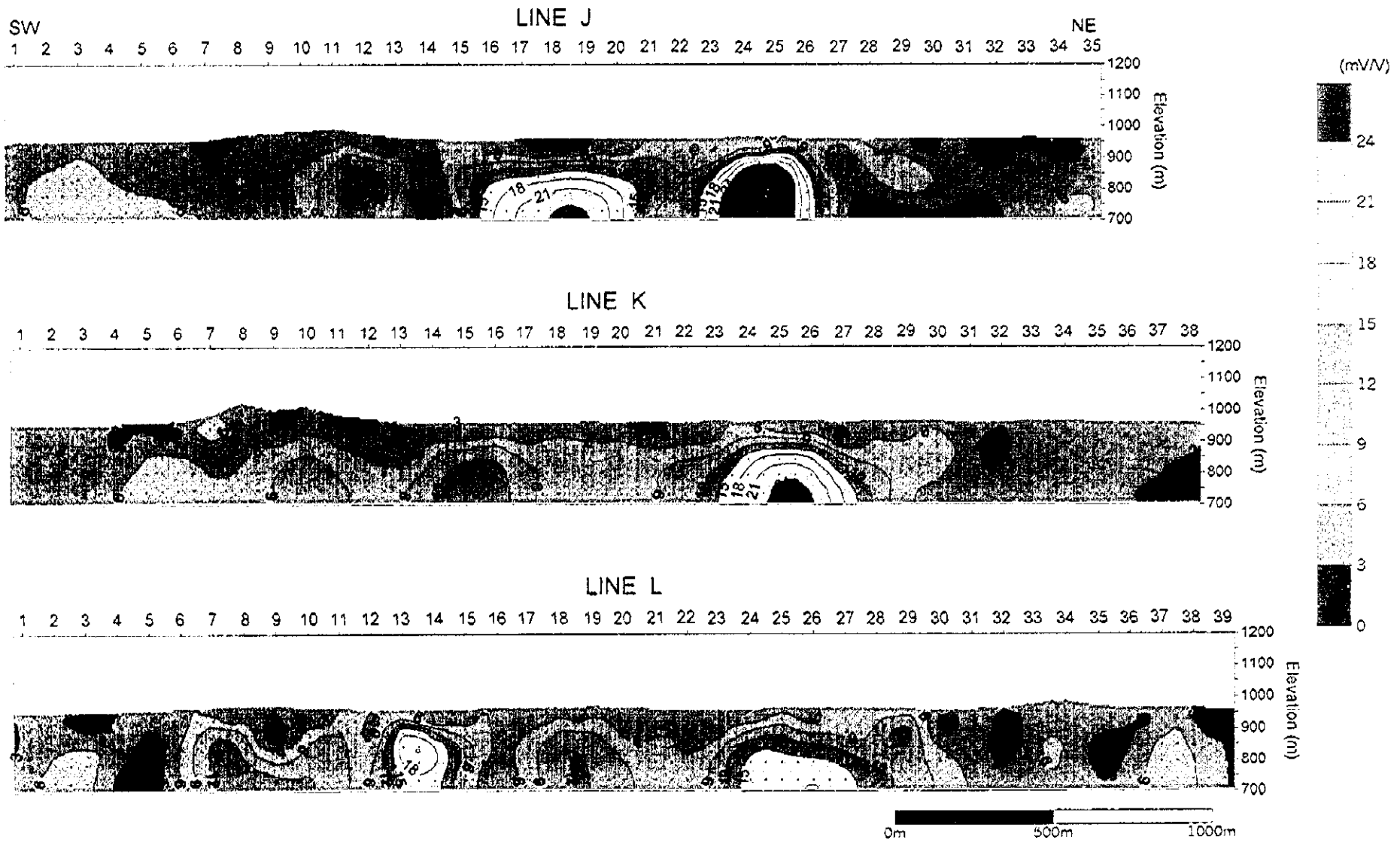

Fig. 2-4-31 Chargeability Section (J, K, L)

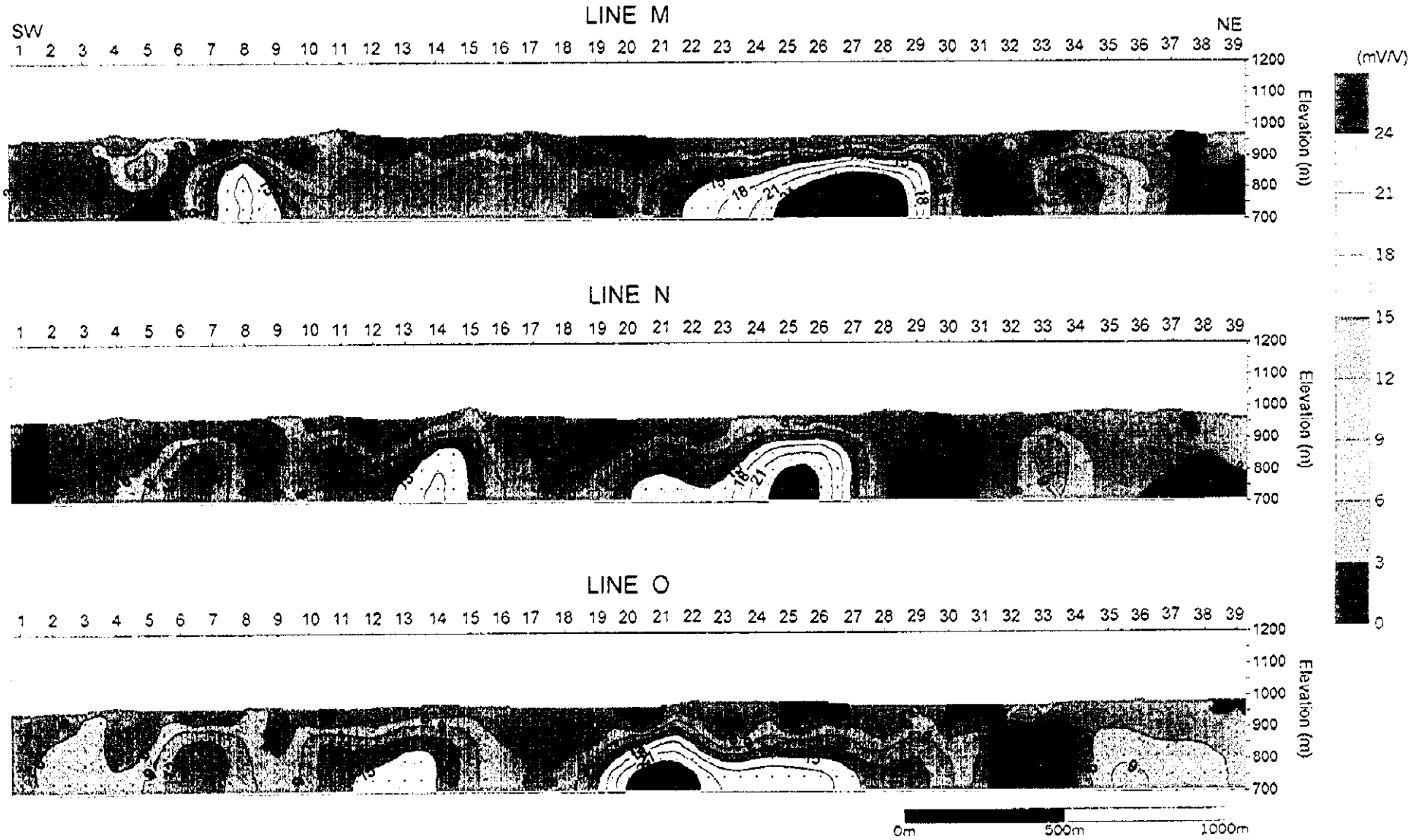

Fig. 2-4-32 Chargeability Section (M. N. O)

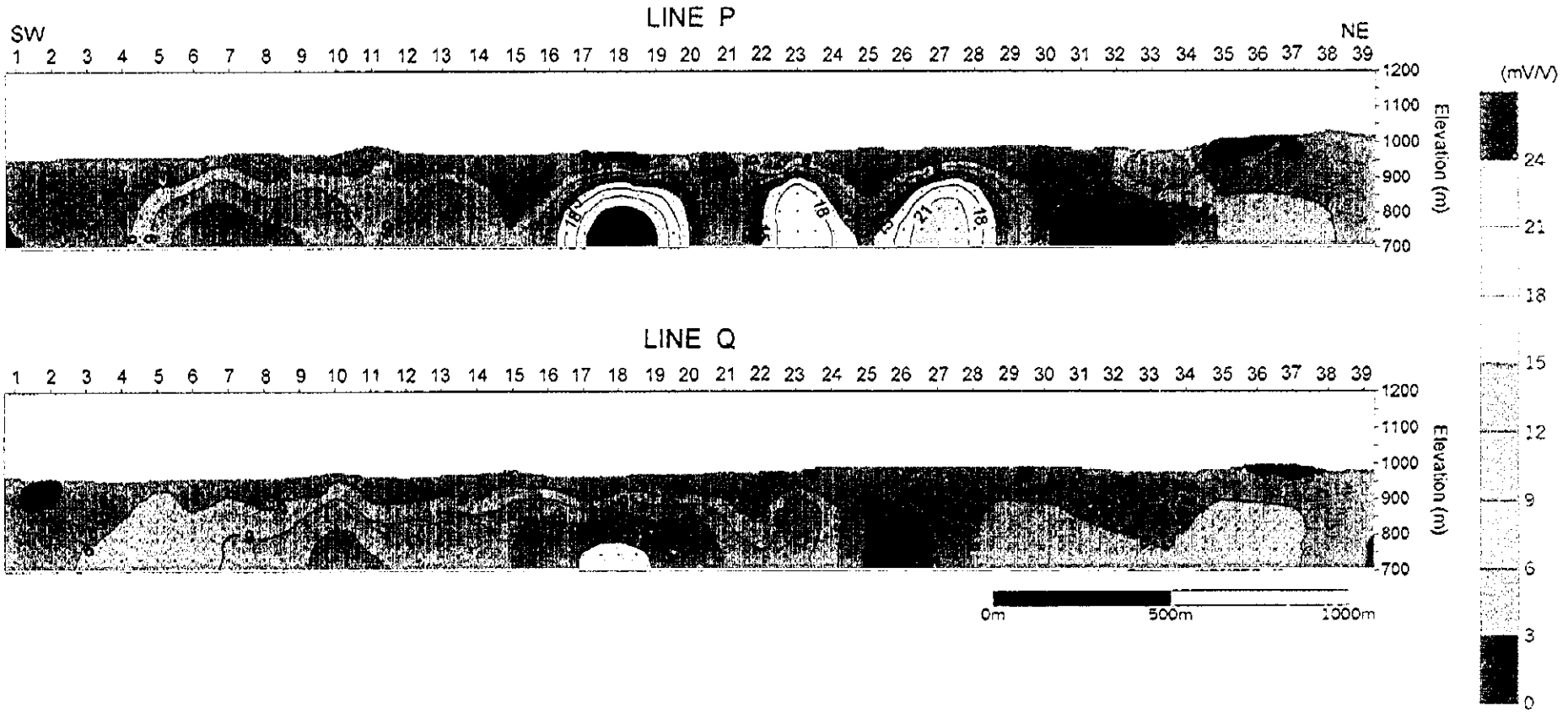

Fig. 2-4-33 Chargeability Section (P, Q)

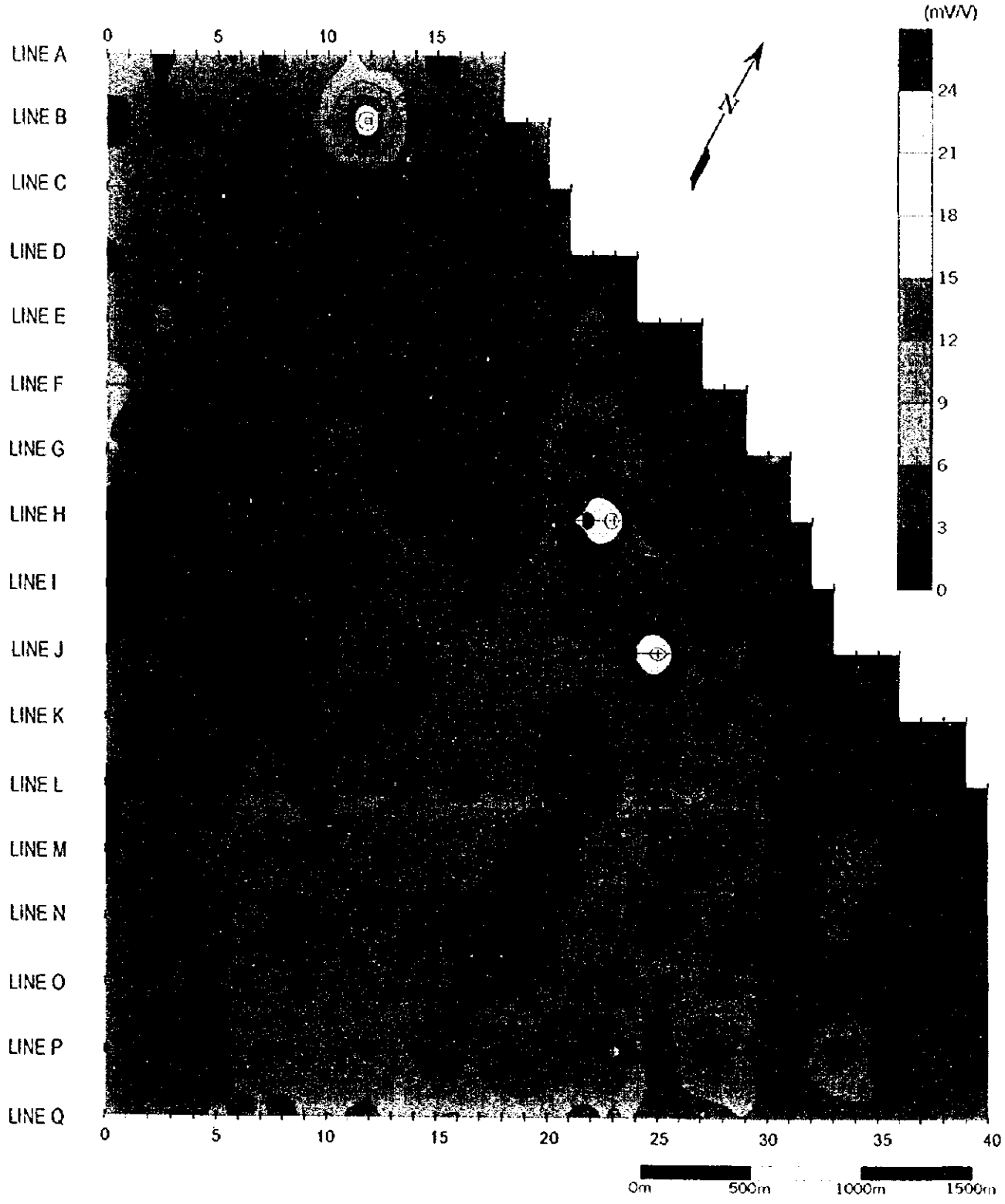

Fig. 2-4-34 Chargeability Map (SL 900m)

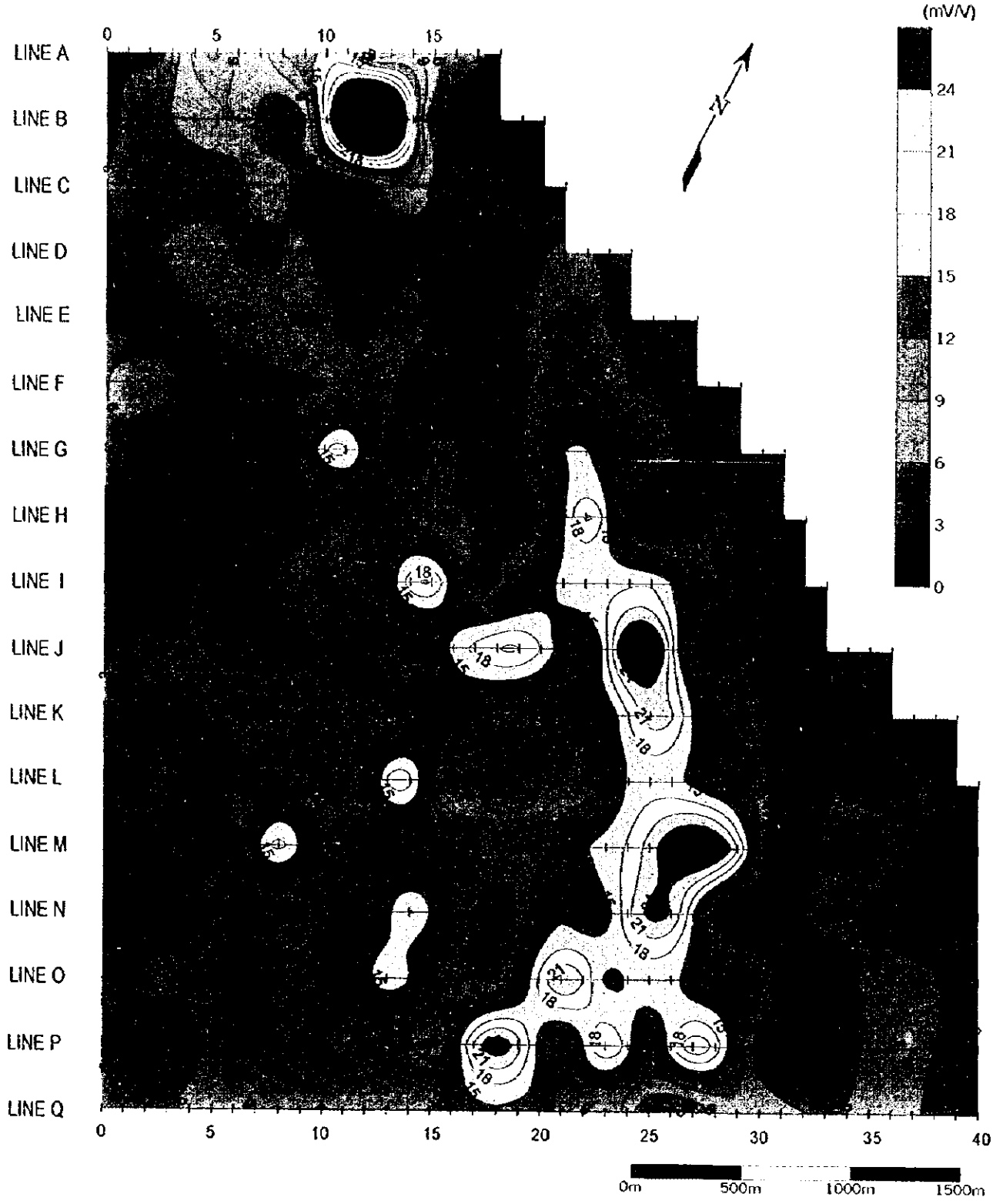

Fig. 2-4-35 Chargeability Map (SL 800m)

4-3-3 Laboratory tests

The results of the laboratory tests are shown in Table 2-4-3. The mean values of resistivity and chargeability for main rocks in this area are as follows.

Rock	Resistivity (ohm-m)	Chargeability (mV/V)
Andesite	26,911	3.8
Dacite	17,112	4.1
Diorite	26,307	3.5

The host rocks (Andesite, Dacite) and the intrusive rock (Diorite) in this area have high resistivity more than 10,000 ohm-m and low chargeability of approximately 4 mV/V. Except for the samples related to mineralization, the other rocks have the similar properties. These properties (high resistivity and low chargeability) of the rock samples accord with the field survey results.

The gossan of the samples related to mineralization measured relatively low resistivity (mean value of 449 ohm-m) and slightly higher chargeability than the host rocks. The ore sample collected from the drilling core (UAD-6) shows high resistivity of approximately 10,000 ohm-m and high chargeability of more than 100 mV/V. This ore sample contains a large amount of network-like sulfide minerals (mainly pyrite)

Table 2-4-3 Results of the Laboratory Tests

Sample No.	Rock Name	Resistivity (ohm-m)	Chargeability (mV/V)	Remarks
1	Altered andesitic tuff	7,139	8.93	Epidotization
2	Andesite	37,186	3.32	brecciated
3	Andesitic arenite conglomerate	28,073	3.48	conglomeratic
4	Andesitic tuff	61,765	2.06	w/dotted epidote
5	Andesitic tuff	33,484	1.47	
6	Andesitic tuff	24,642	3.32	
7	Dacite	34,685	1.81	qtz-feldspar phenocryst, glassy
8	Dacitic crystal tuff	24,208	4.85	Matrix glassy
9	Dacitic crystal tuff	21,823	6.21	yellow epidote veinlets
10	Dacitic crystal tuff	15,106	3.79	qtz-feldspar big crystals
11	Dacitic crystal tuff	6,566	7.56	sheared, glassy
12	Dacitic tuff	9,719	5.53	glassy, hematite weak stain, w/qtz
13	Dacitic tuff	44,731	0.91	
14	Dacitic vitric tuff	22,429	3.11	
15	Rhyodacite	27,956	2.21	qtz phenocryst, groundmass glassy
16	Rhyodacite	4,052	6.05	groundmass glassy
17	Rhyodacitic tuff breccia	18,351	3.81	
18	Greenschist	4,257	3.92	w/Ox-Cu stain, qtz veinlet
19	Greenschist	4,491	3.42	w/Ox-Cu stain
20	Jaspar	58,490	3.18	w/specularite veinlets
21	Jasper (chert)	39,583	2.03	
22	Diorite	34,628	1.94	Microdiorite
23	Diorite	40,338	1.41	Microdiorite
24	Diorite	16,969	3.00	Microdiorite
25	Diorite	11,540	7.26	Microdiorite
26	Diorite	23,455	2.96	Microdiorite, w/epidote, qtz veinlet
27	Diorite	64,956	3.24	w/epidote, porphyritic
28	Quartz diorite (Tonalite?)	26,194	4.00	
29	Quartz diorite(Tonalite?)	21,016	4.10	
30	Epidote-carbonate rock	11,409	6.79	Andesite?
31	Gossan	62	14.80	4/6 Gossan, brecciated
32	Gossan	3,560	2.89	UAD South, silicified
33	Gossan	722	9.75	UAD South
34	Gossan	256	5.67	UAD North, silicified
35	Silicified ore	9,594	115.24	UAD-6 core, Pyrite 20%
36	Slag	50,850	1.17	UAD North

4-3-4 Discussions

(1) Resistivity and Chargeability Features

The laboratory test results and geologic information led to the following resistivity and chargeability features regarding the rocks and geologic structure in this area.

Resistivity

The resistivity of the rocks in this area is high on the whole, judging from the laboratory test. In this area, gravel on the surface and weathered zone under gravel are mainly assumed to form low resistivity. In addition, graphite and fracture zone might cause low resistivity. The laboratory test results for gossan shows that relatively low resistivity is distributed in the shallow and oxidized mineralization zone. However, the laboratory test results show that high resistivity is distributed in deeper mineralization zone containing a large amount of network-like sulfide minerals (mainly pyrite).

Chargeability

The laboratory test results show that the background value of chargeability of this area is low. The sulfide minerals (mainly pyrite) are firstly assumed to cause strong chargeability anomaly. However, the laboratory test results for the gossan show that weak chargeability anomaly is detected where pyrite was oxidized in the shallow zone. A layer containing a large mount of graphite seems to cause strong chargeability anomaly, but it is inferred that lower resistivity is detected, as anomaly becomes stronger.

(2) Relation of IP Survey Results to Geologic Structure and Mineralization

On the basis of the above features, the relation of the IP survey results to geologic structure and mineralization is discussed below.

Relation to Geologic Structure

On the relation of IP anomalies to geologic structure, the following have become clear.

The low resistivity areas distributed in the flat parts on the surface of this area correspond to thick gravel and weathered zone under gravel (maximum about 50m).

Relation to Mineralization

The chargeability anomalies in the deeper zone (SL 800m) are shown in Figure 2-4-36. In this map, the three strong chargeability anomaly zones were extracted around station B-12, station

J-25 and station M-27. The features of every anomaly zone are as follows.

B-12: highest chargeability in the survey area
high resistivity
low resistivity in the shallow zone
NW-SE direction, extending to line A
vertical structure

J-25: high resistivity
NW-SE direction, continuing to line K
vertical structure

M-27: high resistivity
low resistivity in the shallow zone
NW-SE direction, continuing to line K
vertical structure

The above strong chargeability anomalies in the deeper zone reflect the distribution of steep-dipping mineralized zone containing network-like sulfide minerals (mainly pyrite), since they are high in resistivity and vertical in structure. Both anomalous zones of the B-12 and M-27 are expected to be covered by thick gravel and weathered zone under gravel, since low resistivity is distributed in the shallow zone.

In the shallow zone, the weak anomaly zone extracted on lines G to J seems to be attributed to mineralization zone containing oxidized sulfide minerals, since it is relatively low in resistivity and is located in the North Prospect.

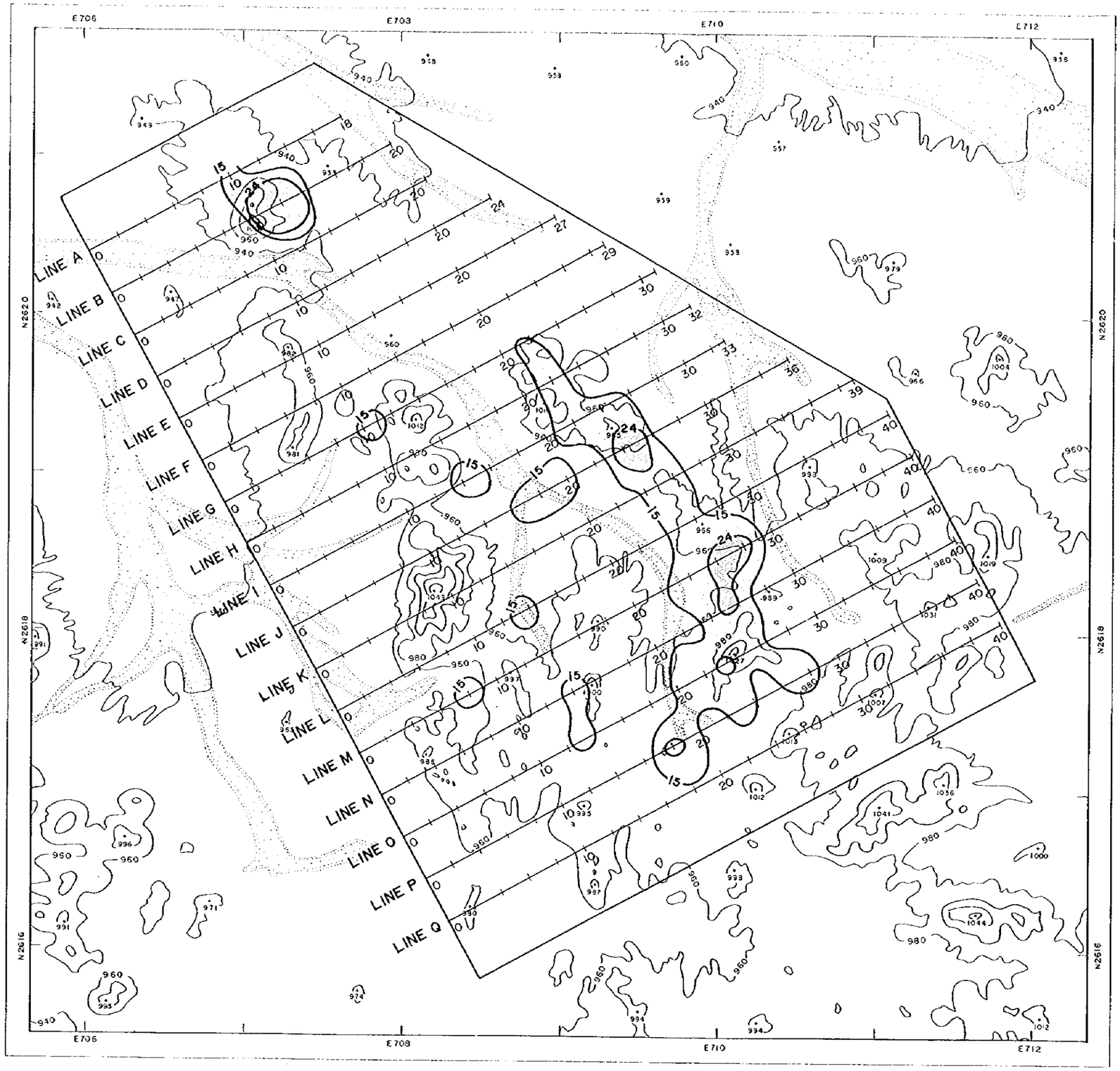

LEGEND

Chargeability

Mx ≥ 24mV/V

15 ≤ Mx ≤ 24mV/V

Scale 1:25,000

0 500 1,000 1,500m

Fig. 2-4-36 Geophysical Anomary Map

PART III CONCLUSIONS AND RECOMMENDATIONS

PART III CONCLUSIONS AND RECOMMENDATIONS

CHAPTER 1 CONCLUSIONS

Analyses and interpretation of existing data, photogeological interpretation, surface geological survey, and IP geophysical survey were carried out in the Umm ad Damar area as the first phase of this project and the following conclusions were obtained.

1. The geology of the survey area consists mainly of; lavas and volcaniclastic rocks of Late Proterozoic rhyodacite, andesite, dacite, and jasper belonging to the Arj Group. This group is intruded by diorite, quartz diorite, tonalite, andesite, dacite, rhyodacite and basalt bodies. These units are covered unconformably by Late Proterozoic andesitic lava and volcaniclastic rocks of the Mahd Group in the western edge of the survey area. The rocks of the Arj Group are regionally chloritized and epidotized, and schistosity is partly developed.

2. Three known prospects, namely Umm ad Damar North, Umm ad Damar South, and 4/6 Gossan occur in the survey area. The mineralized zones of these prospects are products of dissemination to network copper hydrothermal activity, and the zone of the 4/6 Gossan has particularly high Au, Ag, Pb, Zn grade. The existence of seven mineralized zones are inferred in these prospects. They are; five (Nos.1—5) in the North Prospect, one in the South Prospect, and one in the 4/6 Gossan.

3. In the past, geological survey, IP geophysical survey, trenching, and drilling have been carried out for these prospects. Sufficient exploratory work has not been carried out, however, for the lower part and extensions of the mineralized zones. Also the area covered by sand and gravel, which constitutes 60% of the survey area, has not been explored sufficiently.

4. It is concluded from integrated study of the results of the past drilling exploration and present detailed geological survey, that the following zones warrant further exploration; namely under the slag in the North Prospect, western extension of the mineralized zone of the South Prospect, and the lower and southern parts of the mineralized zone of the 4/6 Gossan.

5. Strong chargeability anomalous zones exceeding 24 mV/V were extracted at the following four localities by IP geophysical survey. These zones are at; Jabal Sujarah ("B-12" anomalous zone), southeastern extension of No.3 Mineralized Zone of the North Prospect ("J-

25"), intermediate point between the North and South Prospects ("M-27"), and western edge of the South Prospect ("P-18").

6. Carbonatization is strong near "B-12" and it is located at the intersection of NE-SW and NW-SE faults. Also "B-12" is geologically similar to the Jabal Sayid deposit by the occurrence of jasper, rhyodacite, and other factors. "J-25" is located between NW-SE trending No.3 and No.4 mineralized zones of the North Prospect. "M-27" and "P-18" occur near a NE-SW trending fault, and an oxidized copper-bearing quartz vein and ancient workings are distributed near "M-27". The above four anomalous zones have high resistivity, and it is concluded from various aspects including laboratory tests that the high chargeability anomalies are reflection of the sulfide bodies in the deeper parts.

CHAPTER 2 RECOMMENDATIONS FOR THE SECOND YEAR

2-1 Drilling Exploration

Umm ad Damar North Prospect: Most of the No.2 Mineralized Zone is covered by slag and thus this zone is not well known. Drilling is recommended in this zone for detailed assessment. "J-25" zone is located between the No.3 Mineralized Zone of the Southeast Hill and the No.4 Mineralized Zone of the Southeast Extension and drilling aimed at the lower part of this zone is concluded to be necessary.

4/6 Gossan Prospect: This IP anomalous zone is relatively small, and thus strong and large scale mineralization cannot be anticipated, but the mineralization of this prospect is rich in Au and Ag. It is deemed worthwhile to clarify the mineral potential of this prospect by drilling in the deeper parts of the mineralized zone and in sites south of UAD-13.

2-2 Geophysical Survey

Geophysical surveys in the following zones are considered to be desirable.

"B-12" anomalous zone: This is the largest anomalous zone in the survey area. The elongation and the center of this zone could not be clarified because the IP line interval was large at 300m. Thus drilling cannot be immediately undertaken. IP survey with line interval of about 100m and TEM survey will be the next step of exploration in this zone.

Area including "M-27" and "P-18" anomalous zones: These anomalous zones are inferred to indicate the existence of mineralized zone along the weak line with NE-SW strike, or "P-18" anomalous zone might be the western extension of the mineralized zone of the South Prospect. It is recommended to clarify the continuity and the center of the anomaly by IP geophysical survey with about 100-m line interval and TEM survey.

REFERENCES

REFERENCES

Bowen, R. A. and Smith, G. H., 1981. An Overview Study of the Jabal Sayid District: Technical Record RF-TR-01-2, 72p.

BRGM-OF-07-6 (Open-file Report). Review of Gold Mineralization in the Arabian Schield, 4/6 Gossan, Umm ad Damar District: 10p.

Chinkul, M., 1983. A Study of the Fluid Inclusions and O & H Stable Isotopes at Jabal Sayid and its Bearing on the Mineralization: Unpublished Ms.c. Thesis: Faculty of Earth Sci., King Abdul Aziz University, Jeddah, Kingdom of Saudi Arabia, 174p.

Conraux, J., 1969. Aqiq-Umm ad Damar Drilling Hole Results: BRGM 15p.

DGMR, 1994. Mineral Resources of Saudi Arabia: 322p.

Hakim, H. D. and Chinkul, M., 1989. A Fluid Inclusion Study on Mahd adh Dhahab Gold Deposit, Saudi Arabia: JKAU: Earth Sci., vol.2, pp.51-68.

Harvey T. V., 1984. Ground Geophysical Surveys at the Umm ad Damar Prospect, 1402 to 1404 Program (February 1982 to December 1983): Open-File Report RF-OF-04-12, 44p.

Howes, D. R., 1984. Mineral Exploration of the Umm ad Damar Prospect: 1403-1404 Program (March 1983 to January 1984), Open-File Report RF-OF-04-4, 44p.

Kemp, J., Gros, Y., and Prian, J., 1982. Explanatory Note to the Geologic Map of the Mahd adh Dhahab Quadrangle, Sheet 23E, Kingdom of Saudi Arabia: pp.1-39.

Lewis, P. J. and Martin, G. J., 1983. Mahd adh Dhahab Gold-silver Deposit, Saudi Arabia ,Mineralogical Studies Associated with Metallurgical Process Evaluation: pp.63-72.

Luce, R. W., O'Neil, J. R., and Rye, R. O., 1979. Mahd adh Dhahab: Precambrian Epithermal Gold Deposit, Kingdom of Saudi Arabia: U.S. Geological Survey (Saudi Arabian Project Report 256), 33p.

Ramsom, D. M., 1982. Geology and Mineralization of the Umm ad Damar South Prospect, Jabal Sayid District, Kingdom of Saudi Arabia :Riofinex Geological Mission, 59p.

Ramsom D. M., 1984. Regional Geology of the Umm ad Damar Area and Geology of the North Prospect: Open-File Report RF-OF-04-9, 23p.

RF-1979-9. 6.2 Umm ad Damar: pp.95-98.

Rye, R. O., Hall, W. E., Cunningham, C. G., Czamanske, G. K. Afifi, A. M., and Stacey, J. S., 1982. Preliminary Mineralogic, Fluid Inclusion, and Stable Isotope Study of the Mahd adh Dhahab Gold Mine, Kingdom of Saudi Arabia: Open-File Report USGS-OF-03-4, 26p.

Sabir, H., 1981. Metalogic and Textural Features of Sulfide Mineralization at Jabal Sayid (Saudi Arabia): Bulletin du BRGM Section II, no.1-2/1980-1981, pp.103-111.

Sahl, M. A., 1979. Geology and Mineralization at Umm ad Damar Area: Faculty of Earth Sciences, King Abdul Aziz University, pp.183-221.

PHOTOGRAPHS

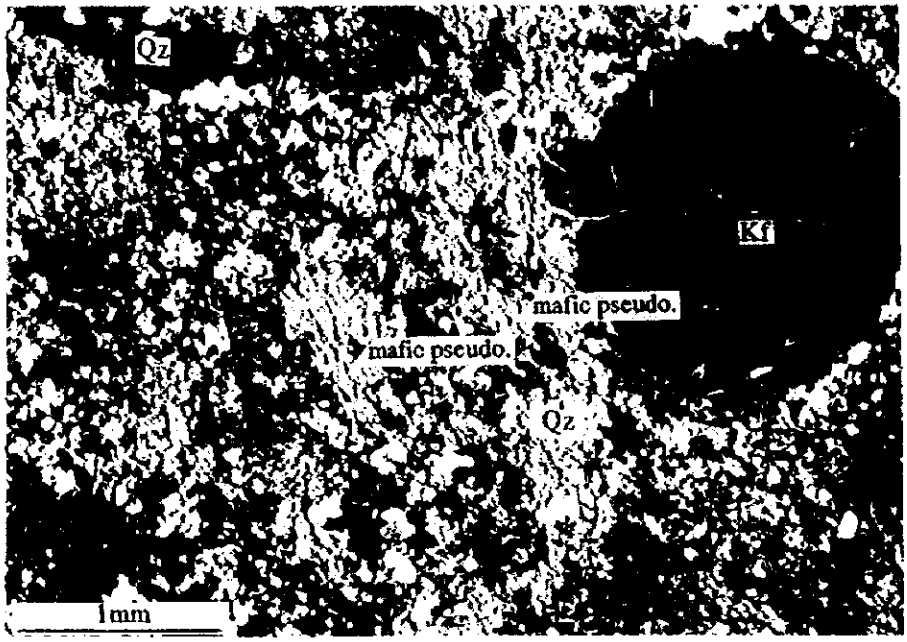

Rock Name: Dacite (Arj Group)
Sample No.: K9022701
Locality: Umm ad Damar North
(Crossed Nicol)

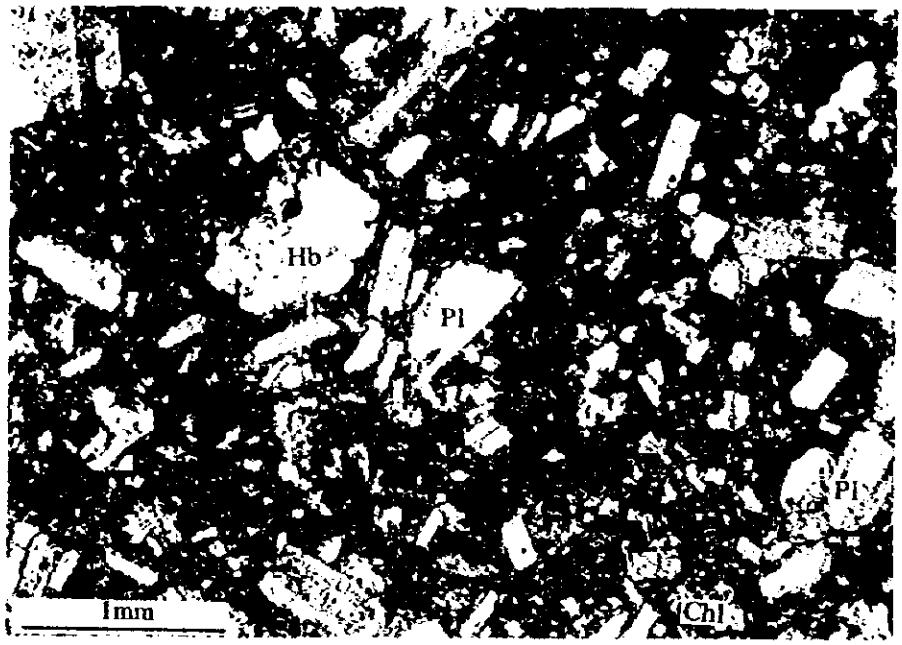

Rock Name: Tuff Breccia (Mahd Group)
Sample No.: M9022013
Locality: Northwest of Jabal Sujarah
(Crossed Nicol)

Abbreviation Pl: Plagioclase, Hb: Hornblende, Chl: Chlorite, Qz: Quartz, Kf: K-feldspar

Photo 1 Photomicrographs of Thin Sections (1)

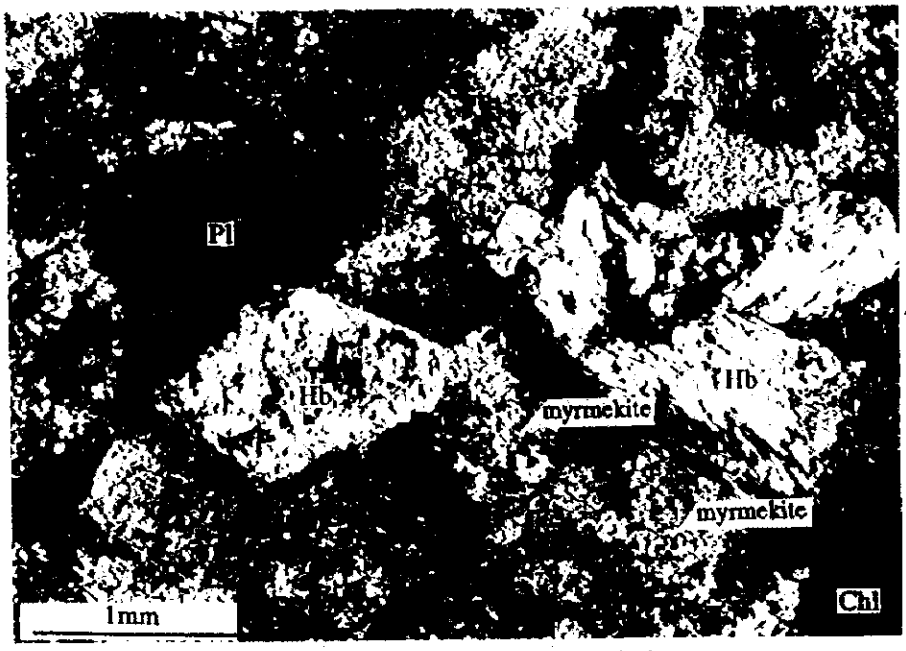

Rock Name: Porphyritic Diorite
Sample No.: K9022005
Locality: Southeastern Margin of Umm ad Damar North Prospect
(Crossed Nicol)

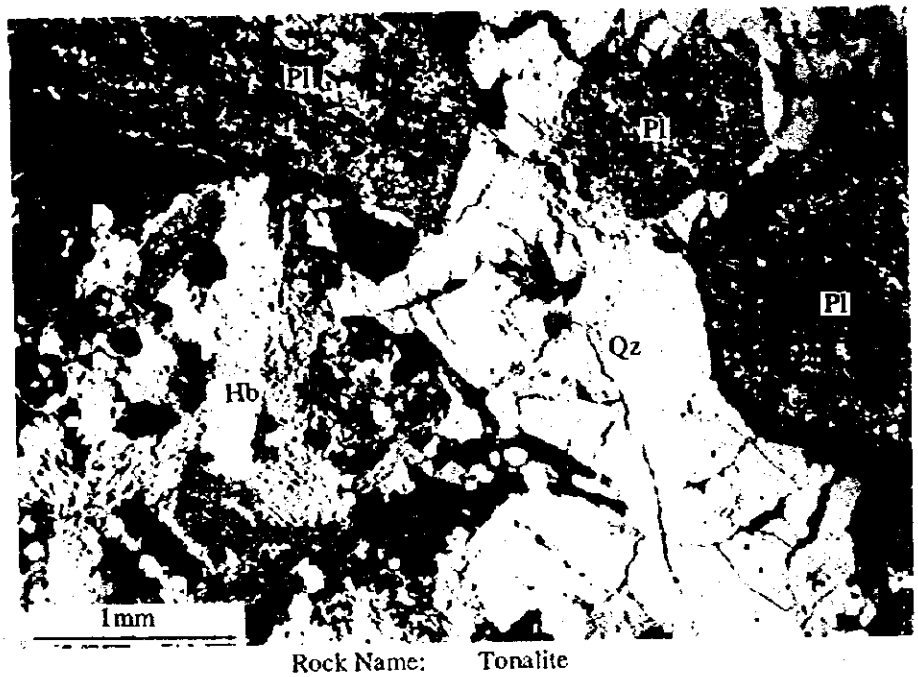

Rock Name: Tonalite
Sample No.: K9021302
Locality: North of Umm ad Damar South Prospect
(Crossed Nicol)

Abbreviation Pl: Plagioclase, Hb: Hornblende, Chl: Chlorite, Qz: Quartz

Photo. 1 Photomicrographs of Thin Sections (2)

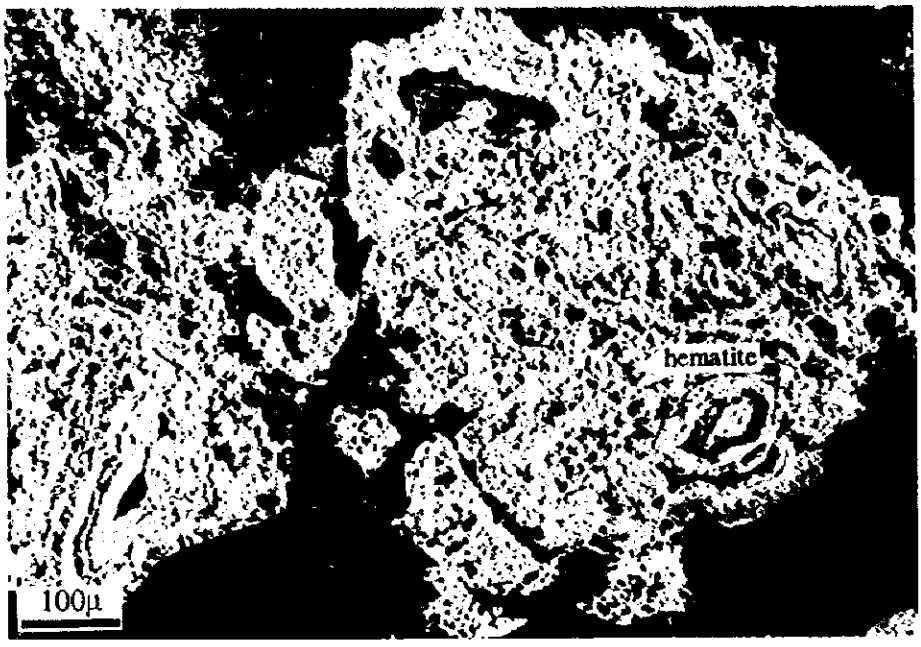

Minerals: Hematite
Sample No.: K9030102
Locality: Umm ad Damar North
(Open Nicol)

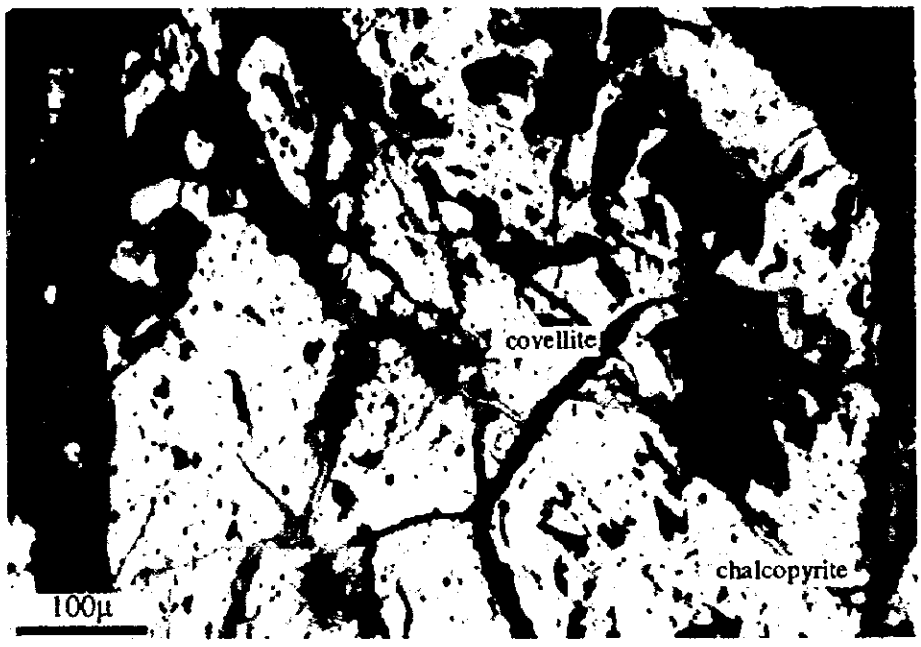

Minerals: Chalcopyrite-Covellite
Sample No.: K9021409
Locality: Southeast Extension of Umm ad Damar South
(Open Nicol)

Photo. 2 Photomicrographs of Ores (1)

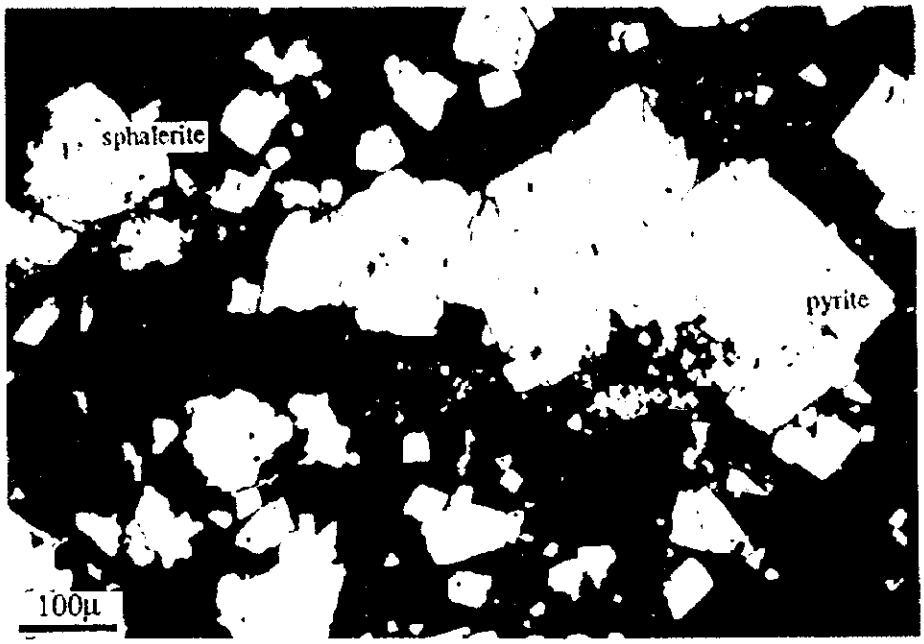

Minerals: Sphalerite-Pyrite
Sample No.: K9030301
Locality: Umm ad Damar North, UAD-6
(Open Nicol)

Minerals: Chalcopyrite-Pyrite-Pyrrhotite
Sample No.: K9030301
Locality: Umm ad Damar North, UAD-6
(Open Nicol)

Photo. 2 Photomicrographs of Ores (2)

Inclusion Type: Liquid-rich Two-phase
Sample No.: K9030307
Locality: Jabal Sayid Deposits

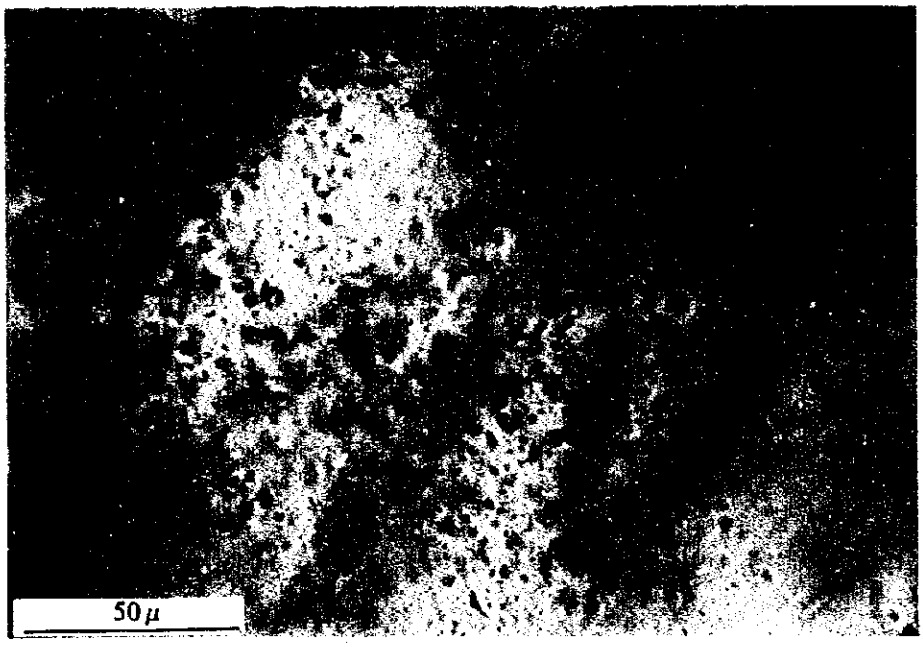

Inclusion Type: Liquid-rich Two-phase
Sample No.: K9030103
Locality: Umm ad Damar North

Photo. 3 Photomicrographs of Fluid Inclusions (1)

Inclusion Type: Liquid-rich Two-phase
Sample No.: K9030301
Locality: Umm ad Damar North, UAD- 6

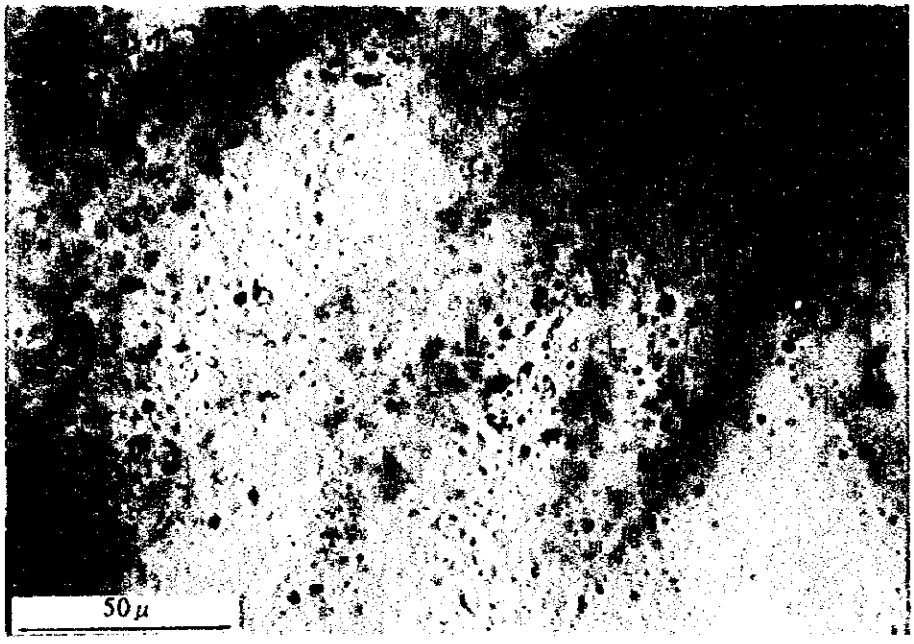

Inclusion Type: Liquid-rich Two-phase
Sample No.: K9022403
Locality: Umm ad Damar South Prospect

Photo. 3 Photomicrographs of Fluid Inclusions (2)